



CircSV2b participates in oxidative stress regulation through miR-5107-5p-Foxk1-Akt1 axis in Parkinson's disease

Quancheng Cheng^{a,1}, Jianwei Wang^{a,1}, Man Li^a, Jinyu Fang^a, Huiru Ding^a, Jieyi Meng^a, Junwei Zhang^b, Xuan Fang^a, Huaicun Liu^a, Chao Ma^c, Chunhua Chen^{a,**}, Weiguang Zhang^{a,*}

^a Department of Human Anatomy and Histology and Embryology, School of Basic Medical Sciences, Peking University Health Science Center, Beijing, 100191, China

^b Department of Liver Surgery, Peking Union Medical College Hospital, Chinese Academy of Medical Sciences and Peking Union Medical College, Beijing, 100730, China

^c Department of Anatomy, Histology and Embryology, Institute of Basic Medical Sciences, Chinese Academy of Medical Sciences, Peking Union Medical College, Beijing, 100730, China

ARTICLE INFO

Keywords:

circSV2b

miR-5107-5p

Foxk1

Akt1

Oxidative stress

ABSTRACT

As a novel type of non-coding RNAs, covalently closed circular RNAs (circRNAs) are ubiquitously expressed in eukaryotes. Emerging studies have indicated that dysregulation of circRNAs was related to neurological diseases. However, the biogenesis, regulation, function, and mechanism of circRNAs in Parkinson's disease (PD) remain largely unclear. In this study, thirty-three differentially expressed circRNAs (DECs) were detected by RNA-sequencing between the MPTP-induced PD mice model and the wild-type mice. Quantitative real-time PCR was used to determine the RNA level of DECs in the striatum (STR), substantia nigra pars compacta (SNpc), and serum exosomes, and it was found that circSV2b was downregulated in PD mice. Then, functional experiments *in vivo* were employed to explore the effect of circSV2b in PD. For the mechanism study, dual-luciferase reporter, fluorescence *in situ* hybridization (FISH), RNA immunoprecipitation (RIP), RNA pull-down, gene editing, and CUT & Tag were performed *in vitro* to confirm that circSV2b directly sponged miR-5107-5p and alleviated the suppression of the expression of the target gene Foxk1, and then positively regulated Akt1 transcription. *In vivo*, the mechanistic analysis demonstrated that circSV2b overexpression resisted oxidative stress damage through the ceRNA-Akt1 axis in PD models. Taken together, these findings suggested that the miR-5107-5p-Foxk1-Akt1 axis might serve as a key target of circSV2b overexpression in PD treatment, and highlighted the significant change of circSV2b in serum exosomes. Therefore, circSV2b might be a novel biomarker for the diagnosis and treatment of PD.

1. Introduction

Parkinson's disease (PD) is the second most common neurodegenerative disease after Alzheimer's disease (AD). The incidence of PD is mainly concentrated in middle-aged and elderly people over 65 years of age, and the incidence rate increases with age [1]. The main pathological change in PD is the degeneration and death of substantia nigra dopaminergic neurons. With the progressive death of neurons, the level of dopamine (DA) in the body gradually decreases. When the DA level in the striatum (STR) is reduced by 80%, clinical symptoms of PD, mainly

tremor, tonicity, motor failure (or reduced motor function), and impaired balance, may occur. Once an individual has symptoms, the loss of dopaminergic neurons in the substantia nigra pars compacta (SNpc) is close to 70% [2]. Therefore, accurate diagnosis is conducive to the prevention and treatment of PD.

The gold standard for the diagnosis of PD is the degeneration of midbrain SNpc neurons and the pathological examination of Lewy bodies (LBs) after death [3]. However, human brain tissue collection and pathological examination are not suitable for clinical diagnosis and screening. Currently, the diagnosis of PD is mainly based on patient symptoms and imaging studies. These assessment methods are

* Corresponding author. Department of Human, Anatomy and Histology and Embryology, School of Basic Medical Sciences, Peking University, Beijing, 100191, China.

** Corresponding author. Department of Human, Anatomy and Histology and Embryology, School of Basic Medical Sciences, Peking University, Beijing, 100191, China.

E-mail addresses: cch@bjmu.edu.cn (C. Chen), zhangwg@bjmu.edu.cn (W. Zhang).

¹ These authors contributed equally: Quancheng, Cheng, Jianwei Wang.

<https://doi.org/10.1016/j.redox.2022.102430>

Received 20 June 2022; Received in revised form 27 July 2022; Accepted 2 August 2022

Available online 12 August 2022

2213-2317/© 2022 The Authors. Published by Elsevier B.V. This is an open access article under the CC BY-NC-ND license (<http://creativecommons.org/licenses/by-nc-nd/4.0/>).

Abbreviations

circRNAs	circular RNAs	ceRNA	competing endogenous RNA
PD	Parkinson's disease	N2A	Neuro-2a
DECs	differentially expressed circRNAs	MPTP	1-methyl-4-phenyl-1, 2, 3, 6-tetrahydropyridine
STR	striatum	AAV	adeno-associated virus
SNpc	substantia nigra pars compacta	HPLC	High Pressure Liquid Chromatography
FISH	fluorescence in situ hybridization	DOPAC	dihydroxyphenylacetic acid
RIP	RNA immunoprecipitation	HVA	hypervanilic acid
AD	Alzheimer's disease	WB	Western blot
DA	dopamine	TH	Tyrosine Hydroxylase
LBS	Lewy bodies	AGO2	Argonaute-2
α -SYN	α -Synuclein	MDA	Malonaldehyde
CSF	cerebrospinal fluid	SOD	Superoxide dismutase
lncRNAs	long non-coding RNAs	GSH-PX	glutathione peroxidase
miRNAs	microRNAs	RISC	RNA-induced silencing complex
		GO	Gene Ontology

subjective and lagging, leading to a high misdiagnosis rate. α -Synuclein (α -SYN) is the main component of LBS, and studies have suggested that changes in the oligomer/total α -SYN ratio in cerebrospinal fluid (CSF) may be an early indicator of PD [4]. However, CSF acquisition is not suitable for large-scale screening. Although α -SYN can also be detected in peripheral blood, as red blood cells are the source of 99% of this protein, its concentration in the blood is strongly influenced by red blood cells [5]. Therefore, in clinical practice, the application of plasma α -SYN as a marker for the diagnosis of PD is limited. Thus, it is extremely important to identify molecular markers that can be used to diagnose PD in peripheral blood. Further analysis of the molecular mechanism of the involvement of novel markers in PD is urgently needed to provide a theoretical basis for the prevention of PD and the development of targeted drugs.

Circular RNAs (circRNAs) are highly conserved and are stable long non-coding RNAs (lncRNAs) that form a covalently closed continuous ring structure through reverse splicing [6]. They are abundantly expressed in the nervous system and have become potential markers and therapeutic targets for neurological diseases [7]. Exosomes are cell-derived vesicles with a diameter of 30–100 nm [8]. Studies have confirmed that exosomes are present in many body fluids, including blood, urine, and saliva [9]. Using exosomes as transports, circRNA can cross the blood-brain barrier to enter the bloodstream and stably exist in the peripheral blood [10]. Therefore, circRNAs released from brain and nerve tissue lesions can be detected in peripheral blood, potentially serving as a novel biomarker to assist in the diagnosis of PD. More interestingly, increasing evidence has shown that circRNAs can act as molecular sponges of microRNAs (miRNAs) through the competing endogenous RNA (ceRNA) mechanism and competitively bind to miRNAs to alleviate miRNA inhibition [11–13]. Therefore, further exploration of the molecular mechanism of circRNA involvement in PD is conducive to better understanding the pathogenesis of PD and developing therapeutic targets.

In this study, we performed rRNA-depleted RNA-seq on SNpc and STR tissues and paired control tissues from a PD mouse model. Then, we analyzed the data using CIRI2 [14], CIRCexplorer2 [15], and DEBKS [16] software. Differentially expressed circRNAs (DECs) were screened out. Total RNA was extracted from the in situ tissues and serum exosomes for Quantitative real-time PCR (qRT-PCR) verification of DECs. Finally, mmu-SV2b-0002 (circSV2b) was selected as the target circRNA. Through an analysis of the characteristics of circSV2b, it was determined that circSV2b is involved in the pathogenesis of PD through the ceRNA mechanism. A bioinformatics database was used to predict the miRNAs targeted by circSV2b and its downstream mRNAs, i.e., miR-5107-5p and Foxk1, respectively.

Foxk1 belongs to the Fox family of transcription factors [17].

Recently, most studies on Foxk1 have focused on tumor-related diseases; there are no reports on its involvement in PD [18,19]. However, studies have found that lncRNAs can regulate the expression of Foxk1 through ceRNAs, thereby participating in disease progression [20,21]. We screened, using CUT & Tag-seq, downstream target genes directly regulated by Foxk1. Because oxidative stress plays an important role in the pathogenesis of PD [22], we further screened the genes associated with oxidative stress downstream of Foxk1 and identified Akt1 as an intermediate regulatory molecule of Foxk1 involved in PD.

To determine the feasibility of circSV2b as a biomarker and the molecular mechanism of its involvement in PD, we tested the hypothesis that circSV2b regulates Foxk1 expression through ceRNA and that Foxk1 acts as a transcription factor to regulate Akt1 expression, thereby participating in PD-related oxidation. Then, the targeting effect of ceRNA was verified by dual-luciferase reporter assays, RNA immunoprecipitation (RIP) assays, and RNA pull-down assays. The regulatory relationship between various molecules was verified by gene editing. In summary, we provide direct evidence that the downregulation of circSV2b in PD reduces the expression of Foxk1 and then accelerates PD progression by reducing Akt1 expression and amplifying oxidative stress damage. In addition, significant changes in circSV2b can be detected in serum exosomes. Therefore, circSV2b can be used as a new target for the diagnosis and treatment of PD.

2. Material and methods

2.1. Mice and cell line

C57BL/6 mice were purchased from the Peking University Health Science Center Department of Laboratory Animal Science. All experiments in this study used 8-10-week-old male mice. The mice were housed under a 12-h light-dark cycle in a thermostatically controlled barrier facility with free access to food. Mice were deeply anesthetized with isoflurane and then sacrificed. For all experiments, a minimal number of animals were used, and the pain was minimized to the best extent possible. This study was approved by the Local Ethics Committee for Animal Research Studies at the Peking University Health Science Center, No. LA2017100.

Neuro-2a (N2A) cells were purchased from Procell (Wuhan, China) and were maintained and stored in accordance with the instructions provided by the supplier. Briefly, N2A cells were maintained in DMEM supplemented with 10% fetal bovine serum (10100139C, Gibco, California, US) and 1% penicillin and streptomycin. The cells were cultured in a humidified incubator containing 5% CO₂ at 37 °C.

2.2. Preparation of the PD mouse model

Mice were housed under standard conditions. After 1 week of adaptation, 1-methyl-4-phenyl-1,2,3,6-tetrahydropyridine (MPTP) (Sigma, Missouri, US) (20 mg/kg) was intraperitoneally injected for 5 consecutive days following a previously described method [23]. The control group was administered the same amount of normal saline.

2.3. Behavioral experiments

The effects of MPTP and adeno-associated virus (AAV)-circSV2b-mediated circSV2b overexpression on motor symptoms in mice were evaluated using a pole-climbing experiment and gait analysis. Starting 6 days before MPTP injection, the same operator trained the mice for the pole climbing and gait tasks at the same time each day for 5 consecutive days. The basal behavioral values of the mice were recorded 1 day before MPTP injection. The behavioral changes were detected at the same time 1 day after the completion of the entire MPTP injection course. The protocols for all tests were similar to those reported in previous studies [24,25]. The instruments were cleaned with 75% ethanol after each test.

- (1) Pole climbing: The mice were acclimatized in the testing room for at least 30 min. As is shown in Figs. S1A and a rod (length, 75 cm; diameter, 1 cm) was wrapped with coarse gauze to facilitate grasping by the animals and was placed in the cage. On the day of the test, the mouse was placed head down on the top of the rod, and the time needed for the mouse to descend to the bottom of the cage was recorded. Timing began when the experimenter released the mouse and stopped when its one hind limb reached the bottom of the cage.
- (2) Gait: The test device was made of a grey acrylic board (3 mm thick) and consisted of a track (10 × 60 × 12 cm) covered with anti-slip white paper and a dark target box (16 × 10 × 12 cm). On the first day of training, the mice were habituated to the device for 2 min. Then, the forepaws and hind paws were painted red and blue respectively with nontoxic dyes, and the mice were trained to run towards the target box. During the experiment, the mice were allowed to run on the track in the same way. Step length and hindfoot width were analyzed, and the footprints near the starting point and the target due to the effect of acceleration or deceleration were excluded. As is shown in Fig. S1B, step length was measured as the average distance between each forepaw and hind paw footprint. Step width was measured as the average distance between the left and right footprints of each forepaw and each hind paw. At least 4 values were measured for each parameter in each experiment.

2.4. High pressure liquid chromatography (HPLC) detection

Mice in each group were sacrificed and their brains were rapidly removed, the STR was dissected out and homogenized in 0.1 mM oxalic acid. The homogenates were centrifuged at 15,000×g for 40 min at 4 °C. The supernatants were filtrated through a 0.22-μm-syringe filter. The concentrations of DA, 3,4 dihydroxyphenylacetic acid (DOPAC), and hypervanilic acid (HVA) were determined using HPLC analysis as described above [26]. To quantify the sample peaks, each chemical was compared to external standards (DA hydrochloride, DD0177; DOPAC, DE0034; HVA, DG0021. Desite, Chengdu, China).

2.5. Western blot (WB)

SNpc and STR tissues and adherent cells were placed in prechilled RIPA buffer containing protease and phosphatase inhibitors, followed by sonication and centrifugation (10,000 g, 10 min, 4 °C) to remove residual tissue. The concentration of protein in the supernatant was

determined by the BCA method. A sample buffer was added to every 5 μg of protein, and the samples were boiled at 100 °C for 5 min, separated by 8% sodium dodecyl sulfate-polyacrylamide gel electrophoresis (SDS-PAGE), and transferred to an NC membrane. At room temperature, the membranes were blocked with TBST solution containing 5% skim milk powder for 120 min, and then, the primary antibody was added and incubated at 4 °C overnight. The membrane was washed 3 times with TBST for 15 min. Then, the enzyme-labeled secondary antibody was incubated at room temperature for 120 min. After 3 washes (15 min each) with TBST, the bands were visualized using an enhanced chemiluminescence solution. Image J software was used for the greyscale analysis of the scanned WB images. The antibodies used in the experiment are listed in Table 1.

2.6. Immunohistochemistry (IHC) and immunofluorescence (IF)

IHC and IF were performed on 5-μm-thick brain sections or cells. Mice were perfused with phosphate buffered saline (PBS) and 4% paraformaldehyde (PFA), and the brain was removed and fixed in 4% PFA overnight. After dehydration in an alcohol gradient and clearance with xylene, the brains were embedded in paraffin and sectioned. Adherent cells were digested, centrifuged, and fixed with 4% PFA for 20–30 min and then embedded in paraffin and sectioned. After the paraffin sections were deparaffinized with xylene, gradient alcohol hydration was performed. The EDTA antigen retrieval solution was added, and the sections were heated at a constant temperature of 95 °C for 15 min. The sections were then blocked with PBS containing 10% goat serum and 0.2% Triton X-100 and then incubated with TH or Foxk1 antibody overnight at 4 °C. After washing with PBS for 3 times, the sections were sequentially incubated with the appropriate biotinylated secondary antibody and avidin-biotin complex for 30 min each; DAB peroxidase substrate was used for development, and images were captured under a light microscope. The results were analyzed using Image J software. For TH and Foxk1 double labeling, in the first round, the sample was incubated with the TH antibody and developed with DAB, and the sections were then heated in boiling water for 8 min to inactivate the peroxidase. Then, in the second round, the sample was incubated with the Foxk1 antibody and developed with DAB containing metallic nickel (abs9211, Absin, Shanghai, China). The first half of the immunofluorescence staining procedure was consistent with that of the immunohistochemistry procedure. After incubation with the primary antibody, the sample was incubated with Alexa Fluor 488- or 594-conjugated secondary antibody at room temperature for 120 min. Analysis was performed using a fluorescence microscope. The antibodies used in the experiment were listed in Table 1.

2.7. RNA extraction, library preparation for RNA-seq, and sequencing data analysis

A FastPure Cell/Tissue Total RNA Isolation Kit (RC101, Vazyme, Nanjing, China) or MiPure Cell/Tissue miRNA Kit (RC201, Vazyme,

Table 1
Antibodies used in this study.

Antibodies	Source/Cat. No.	Host	Dilution
Tyrosine Hydroxylase (TH)	Millipore (AB152)	Rabbit	1:2000 (WB) 1:500 (IHC, IF)
Akt1	Proteintech (80457-1-RR)	Rabbit	1:1000 (WB)
Foxk1	Abcam (ab85999)	Rabbit	1:1000 (WB) 1:300 (IHC) 1:50 (CUT&Tag)
Argonaute-2(AGO2)	Abcam (186733)	Rabbit	1:200 (IF) 5 μg/tube (RIP)
GAPDH	Bioss (bsm-0978 M)	Mouse	1:1000 (WB)

Nanjing, China) was used to extract total RNA or miRNA of SNpc, STR, and serum exosome following the manufacturer's instructions. Total RNA in the nuclear and cytoplasmic fractions of the SNpc was extracted using the PARIS™ Kit (AM1921, Invitrogen, California, US). Before extracting total RNA from serum exosomes, 5 fmol/μL cel-miR-39 (59000, Norgen, Thorold, Canada) was added to each sample.

An rRNA-depleted RNA library was constructed and sequenced by Annonoad Gene Technology (Beijing, China). rRNA was removed using the Ribo-Zero rRNA Removal Kit (MRZG12324, Illumina, California, US). A total of 3 μg of RNA was used as the input material for each sample. The library was generated after sequencing using an Illumina HiSeq X platform, and paired-end reads of 150 bp were obtained. The data were analyzed using CIRI2, CIRCexplorer2, and DEBKS software.

mRNA-seq and data processing were completed by Personalbio (Shanghai China). The mRNA was enriched with oligo (dT)-containing magnetic beads, and the cDNA library was obtained by PCR enrichment. After library quality control, sequencing was performed using the Illumina platform.

2.8. qRT-PCR analysis

Total RNA (500 ng) was reverse transcribed into complementary DNA (cDNA) using the HiScript®III RT Strand SuperMix for qPCR (+gDNA wiper) (R323, Vazyme, Nanjing, China). For each circRNA and mRNA, 2 upstream and downstream primers were designed. qRT-PCR was performed using the ChamQ™ Universal SYBR® qPCR Master Mix (Q711, Vazyme, Nanjing, China) on an ABI7500 system following the manufacturer's procedure, with β-actin as the internal reference gene. The miRNA detection was performed with All-in-One™ miRNA qRT-PCR Detection System 2.0 (QP116, GeneCopoeia, Maryland, US). The primers for the 3 miRNAs were purchased from GeneCopoeia (Maryland, US), and the internal reference was U6. The other primers used in the experiment were listed in Table 2. The primers of 33 circRNAs were listed in Table S2 (The 33 circRNAs were numbered in Table S1).

2.9. Extraction of serum exosomes

Blood was collected from the angular vein and stored at room temperature for 60–120 min. After coagulation, the blood was centrifuged at 1500×g at 4 °C for 10 min. The upper layer of the yellow transparent liquid was serum. The serum was centrifuged at 2000×g for 30 min at room temperature to remove residual cells and debris and placed on ice until use. The serum and VEX® Exosome Isolation Reagent (R602, Vazyme, Nanjing, China) were thoroughly mixed at a ratio of 5:1 following the manufacturer's instructions and then allowed to stand at 4 °C for 30 min. After centrifugation at 10,000×g for 5 min at room temperature, the supernatant was discarded; the pellet (exosomes) was retained.

2.10. Fluorescence in situ hybridization (FISH)

The location of circSV2b, miR-5107-5p, and mRNA Foxk1 in brain tissue or N2A cells was observed via FISH. A CY3-labeled circSV2b probe, FAM-labeled miR-5107-5p, and DIG-labeled Foxk1 were designed and synthesized by BIOSOURCE (Beijing, China). The probes

Table 2
Primers used in this study.

Primer	Forward Primer 5'-3'	Reverse Primer 5'-3'
circSV2b	TTACTACGGCCTGACGGTGT	GGCTTCATCATGTTTGCCCA
linear SV2b	AGAGCTCAACCGGAACCTGG	GGCCCATCACACAGTACAA
β-Actin	TGTTACCAACTGGGACGACA	GGGGTGTGAAGGTCTCAAA
Foxk1	GACCTAAGCATGGCCTGTG	AACCGGAAGGTGATTGTTG
Akt1	GCCGCCTGATCAAGTTCTCC	TTCAGATGATCCATGCGGGG

were used for overnight hybridization following the manufacturer's instructions. Images were collected using a Zeiss LSM710 confocal laser scanning microscope. The probes used in the experiment are listed in Table 3.

2.11. Agarose gel electrophoresis

Ten micrograms of RNA were incubated with RNase R (P0301, Genesee, Guangzhou, China) at 37 °C for 30 min. Then, the treated RNA was reverse transcribed using different primer pairs, amplified by PCR, and electrophoresed.

The cDNA and gDNA PCR products were electrophoresed in 2% agarose gel and TAE buffer at 100 V for 30 min. The bands were observed by UV irradiation.

2.12. circSV2b-overexpressing mice construction

Dopaminergic cell-specific circSV2b-overexpressing mice were created by injecting adeno-associated virus (AAV) TH-mmu-circ-0001583-ZsGreen (Hanbio, Shanghai, China) into the SNpc.

Stereotaxic injection. Vector solution was bilaterally injected within the SNpc region using a 0.2 mm-gauge stainless steel injector connected to a 5 μl Hamilton syringe. In all experimental groups, the AAV was injected in a volume of 1 μl/side at a rate of 0.2 μl/min. The stereotaxic coordinates used (flat skull position) were: AP = −3.2 mm; ML = ± 1.2 mm, DV = −4.6 mm relative to the bregma, according to the atlas of Paxinos and Franklin (2001). Only animals with correct injection placements, verified by analysing immunofluorescence staining of consecutive coronal brain sections, were included in the statistical analysis transgene expression of circSV2b.

2.13. Design and transfection of overexpression and interference expression plasmids and oligonucleotides

The plasmids were constructed by Hanbio (Shanghai China).

To construct a stable circSV2b overexpression vector, we synthesized full-length circSV2b cDNA and cloned it into the pCDNA3.1-circRNA-EF1-ZsGreen overexpression vector, which contains a front and back circular frame to promote RNA circularization. An empty vector without the circSV2b sequence was used as a negative control.

The siRNA and shRNA sequences of the circSV2b gene and the sequences of the control vector are shown in Table S3. The selected

Table 3
Probes used in this study.

Number	Name	Sequence	Marker
1	Foxk1	GGGATTGTGGCAAATGCTATGGTGGGCTTCTCT (ttt CATCATCAT ACATCATCAT)30+- tt ATGATGATGT ATGATGATGT	DIG (FISH)
2	miR-5107-5p	TGTCCTGCCTCCTCTGCCCA(ttt CATCATCAT ACATCATCAT)30+- tt ATGATGATGT ATGATGATGT	FAM (FISH)
3	circSV2b	TGCTGAAGCCCCAGCTTATCGTTTCAAAAG(ttt CATCATCAT ACATCATCAT)30+- tt ATGATGATGT ATGATGATGT	CY3 (FISH)
4	circSV2b	TGCTGAAGCCCCAGCTTATCGTTTCAAAAG	5' biotin (RNA pull down)
5	Foxk1	GGGATTGTGGCAAATGCTATGGTGGGCTTCTCT	5' biotin (RNA pull down)

interference vector was pCDNA3.1-U6-CMV-ZsGreen.

MiR-5107-5p mimics or miR-5107-5p inhibitors were directly used to regulate the expression of miR-5107-5p, which were provided by Geneseeed (Guangzhou, China), and the sequence is listed in Table S3.

We synthesized the full-length *foxk1* sequence and cloned it into the vector pCDNA3.1-CMV-MCS-3flag-EF1-ZsGreen-T2A-Puro. An empty vector without the *foxk1* sequence was used as a negative control.

The siRNA and shRNA sequences of the *foxk1* gene and the sequences of the control vector are shown in Table S3. The selected interference vector was pCDNA3.1-U6-NC-CMV-ZsGreen-T2A-PURO.

2.14. Stable transfection was performed in N2A cells by advance transfection reagent (AD600150, Zeta life, California, USA)

2.14.1. RIP

RIP was performed in accordance with the instruction of the RIP kit (P0101, Geneseeed, Guangzhou, China). After transfection with a miR-5107-5p mimic or negative control, N2A cells were lysed in a complete RIP lysis buffer. Then, the cell extracts were incubated with magnetic beads conjugated with anti-AGO2 or anti-IgG antibodies at 4 °C for 6 h. The magnetic beads were washed and incubated with proteinase K to remove protein. Finally, the isolated RNA was extracted using Trizol Reagent, after which qRT-PCR was performed.

2.15. RNA pull-down assay

Biotinylated circSV2b and Foxk1 (RuiBiotech, Beijing, China) pull-down assays were performed as described earlier [27]. In brief, 1×10^7 N2A cells were harvested, lysed, and sonicated. The probe was incubated with streptavidin magnetic beads (Geneseeed, Guangzhou, China) at 25 °C for 2 h to generate probe-coated beads. The cell lysates were incubated with the probe-coated beads mixture at 4 °C overnight. After washing with the wash buffer, the RNA-protein complexes bound to the beads were eluted and purified with Trizol Reagent for WB analysis to detect AGO2 enrichment. The sequences of probes were listed in Table 3.

2.16. Dual luciferase reporter assay

The circSV2b and Foxk1 3'UTR sequences and their corresponding mutants were designed and synthesized by Geneseeed (Guangzhou, China) and then inserted into the dual luciferase reporter vector psi-CHECK2; the products were named circSV2b-wt, circSV2b-mut, Foxk1-wt, and Foxk1-mut. All plasmids were cotransfected with miR-5107-5p mimics or inhibitors into N2A cells. Then, the relative luciferase activity was detected using the Double-Luciferase Reporter Assay Kit (TransGen, Beijing, China) following the manufacturer's protocol.

2.17. CUT & Tag-seq

Concanavalin A-attached magnetic beads were used to bind the cells, and the cell membrane was permeabilized with digitonin. Mediated by the Foxk1 antibody, the corresponding secondary antibody, and protein A/G, the transposon fused with protein A/G accurately targeted and cleaved the DNA sequence near the Foxk1 protein. Adaptor sequences are added to both ends of the cleaved fragments during transposon cleavage. After PCR amplification, the sequence can be directly used for high-throughput sequencing. In accordance with the instruction manual, the following procedures were performed in order: cell collection, primary antibody binding, secondary antibody binding, hyperactive pA/G-transposon binding, fragmentation, DNA extraction, library amplification, PCR product purification, library quality control, and sequencing. Sequencing and data analysis were performed by Frasergen (Wuhan, China).

2.18. Detection of oxidative stress-related molecules

Malonaldehyde (MDA) was detected by an Enzyme-linked immunosorbent assay (ELISA). Superoxide dismutase (SOD) and glutathione peroxidase (GSH-PX) were detected using biochemical reagent kits (BC0175, BC1195, Solarbio, Beijing, China).

MDA: Following the instruction of the Mouse MDA ELISA Kit (EM1723-1, FineTest, Wuhan, China), the sample or standard competed with a fixed number of targets on a solid-phase carrier to obtain the target biotinylation site for antibody detection. Excess conjugated and unbound samples or standards were washed off of the plate, and enzyme-labeled streptavidin was added to each microplate well, followed by incubation. Then, a TMB matrix solution was added to each well. The enzyme-substrate reaction was terminated by adding sulfuric acid solution, and the color change was measured by spectrophotometry at a wavelength of 450 nm. Then, the concentration of the target molecule in the sample was determined by comparing the OD value of the sample with the standard curve.

SOD: O_2^- can reduce nitroblue tetrazolium to produce blue formazan (absorption at 560 nm); SOD can remove O_2^- , thereby inhibiting the formation of formazan, and thus, the darker is the blue color of the reaction solution, the lower is the SOD activity, and vice versa. In accordance with the manufacturer's instructions, the liquids in the measuring tube, control tube, and blank tube were mixed well. After incubation in a 37 °C water bath for 30 min, the absorbance of each sample was measured at 560 nm.

GSH-PX: GSH-PX catalyzes H_2O_2 to produce GSH. GSH reacts with 5, 5'-dithiobis-(2-nitrobenzoic) acid (DTNB) to produce 2-nitro-5-mercaptobenzoic acid and GSSG. 2-nitro-5-mercaptobenzoic acid is a yellow product with a maximum light absorption at a wavelength of 412 nm. Following the manufacturer's instructions, a gradient tube, sample tube, and blank tube (standard curve) were set up. The liquid in each tube was mixed well and then allowed to stand for 2 min. The absorbance at 412 nm was measured.

2.19. Statistical analysis

Data are expressed as the mean \pm s.e.m. with at least three biologically independent experiments. Representative morphological images were taken from at least three biologically independent experiments with similar results. The unpaired two-tailed Student t-test was used for comparison between two groups, and one-way ANOVAs followed by Bonferroni's post hoc test was used for multi-component comparisons. All data were analyzed using the appropriate statistical analysis methods, as specified in the figure legends, with the SPSS software (version 19.0). Significance was accepted at * $P < 0.05$, ** $P < 0.01$.

3. Results

3.1. MPTP successfully induces the development of PD in mice

With reference to previous reports [23], we intraperitoneally injected the MPTP solution for 5 consecutive days to create a PD mouse model. After the model was constructed (Fig. S2), behavioral tests were performed, and samples were collected. As seen in Fig. 1A–C, MPTP reduced DA and its metabolites (DOPAC and HVA) levels in the STR ($P < 0.01$). Both pole-climbing experiments and gait analysis revealed that MPTP treatment impaired motor balance in mice ($P < 0.01$, Fig. 1D–F). MPTP treatment reduced TH expression in the SNpc and STR and damaged dopaminergic neurons ($P < 0.01$, Fig. 1G–J). These results indicate that MPTP attenuates dopamine synthesis, destroys nigrostriatal function, and induces the motor symptoms of PD.

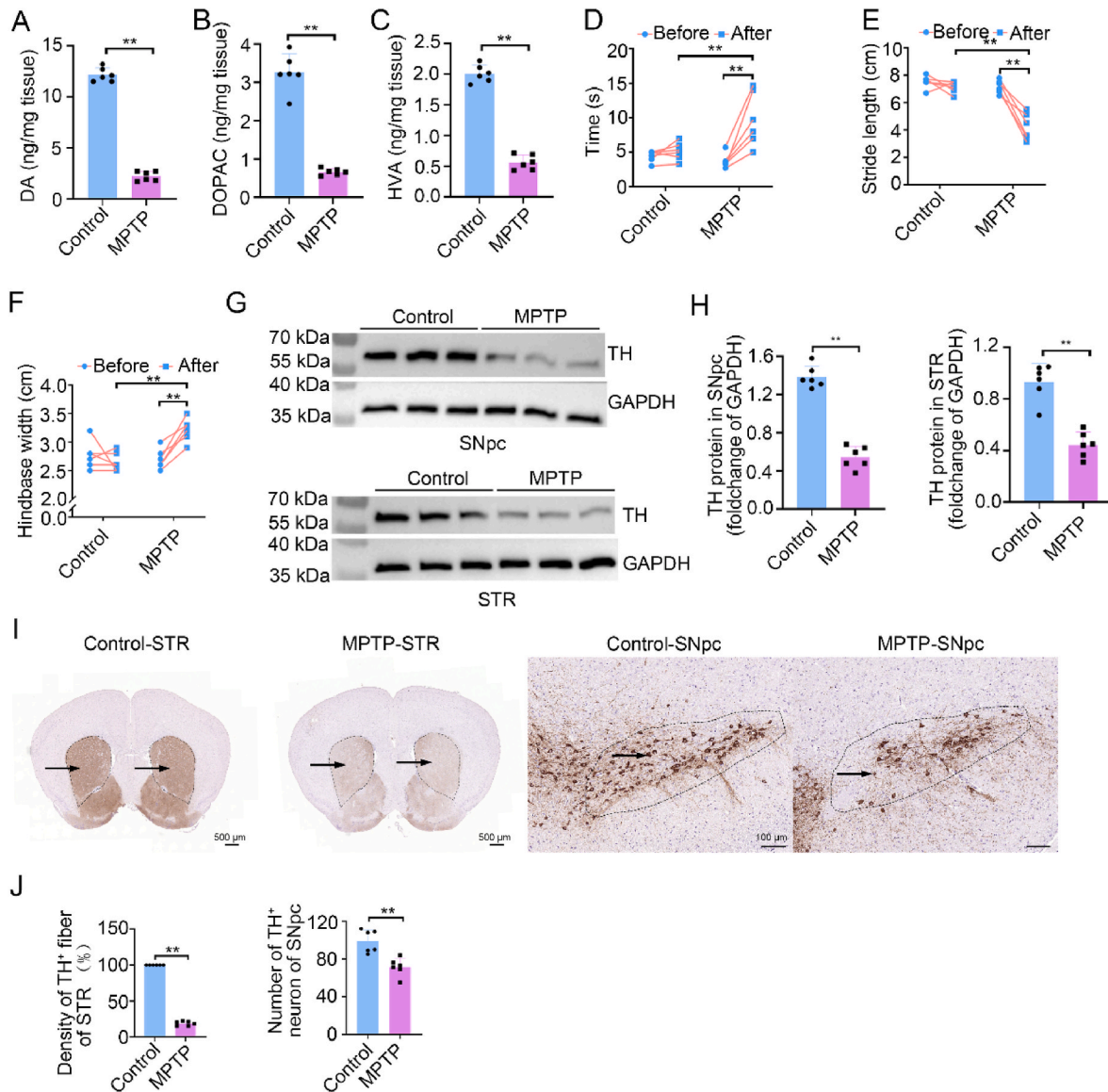


Fig. 1. Validation of MPTP-induced mouse PD model. **A, B and C** represent the content of DA, DOPAC, and HVA in STR, respectively. The content of DA and its metabolites in MPTP group decreased ($P < 0.01$). The result is the amount of DA, DOPAC, and HVA per mg of tissue. Data are mean \pm s.e.m.; $n = 6$. **D, E and F** represent time to descend pole, stride length, and hindbase width of gait analysis, respectively. MPTP group had longer time, smaller stride length and larger hindbase width ($P < 0.01$). Data are mean \pm s.e.m.; $n = 6$. **G and H** represent protein levels of TH and GAPDH in SNpc and STR. The expression of TH protein in MPTP group was decreased ($P < 0.01$). Data are mean \pm s.e.m.; $n = 6$. **I and J** were representative photomicrographs and unbiased stereological counts of TH immunohistochemical staining in STR and SNpc. Both TH⁺-fiber content (in STR) and TH⁺-cell number (in SNpc) of MPTP group were decreased ($P < 0.01$). The black arrows indicate the location of TH⁺ fibers or TH⁺ neurons. Scale bar, 500 μ m for STR, 100 μ m for SNpc. Data are mean \pm s.e.m.; $n = 6$. The one-way ANOVAs were used for statistical analysis followed by Bonferroni's post hoc test. ** $P < 0.01$.

3.2. Screening and identification of circSV2b as a diagnostic and therapeutic target for PD

The rRNA-depleted RNA-seq data of SNpc and STR tissues were analyzed using CIRI2, CIRCexplorer2, and DEBKS software. Because there was very little SNpc tissue, we performed risk sequencing; no DECs were found in SNpc tissue. In contrast, 8 upregulated and 25 downregulated circRNAs were found in STR tissue (Fig. S3). The expression of 33 DECs in the 2 groups is shown in Fig. 2A, and for the ease of description, the 33 circRNAs were numbered (Table S1). The presence of these 33 circRNAs in STR tissue was verified by qRT-PCR. The results indicated that among the 25 downregulated circRNAs (RNA-seq), 14 were downregulated, 8 were upregulated, 2 were unchanged, and 1 was undetected; among the 8 upregulated circRNAs (RNA-seq), 5 were upregulated, 2 were downregulated, and 1 was undetected (Fig. 2B).

Nineteen circRNAs whose RNA-seq data (in STR) were consistent with the qRT-PCR results (in STR) were assessed (qRT-PCR) in SNpc and serum exosomes (Fig. 2C). CircRNA #3, i.e., circSV2b, whose RNA-seq (in STR) and qRT-PCR validation (in STR, SNpc, and serum) results were consistent, was selected as the target of this study (Fig. 2C). FISH further confirmed that circSV2b expression in the SNpc and STR was downregulated after MPTP treatment (Fig. 2D).

CircSV2b is derived from the SV2b gene on mouse chr7 (qD1) and is formed from exons 5–9 by head-to-tail splicing after transcription (Fig. 2E). However, head-to-tail splicing may not only result from reverse splicing but may also result from genome rearrangement [27]. To rule out this possibility, convergent primers for SV2b mRNA and special divergent primers to amplify circSV2b were designed. cDNA and gDNA were extracted from SNpc tissue and analyzed by PCR and agarose gel electrophoresis. A 320-bp circSV2b product was detected in the

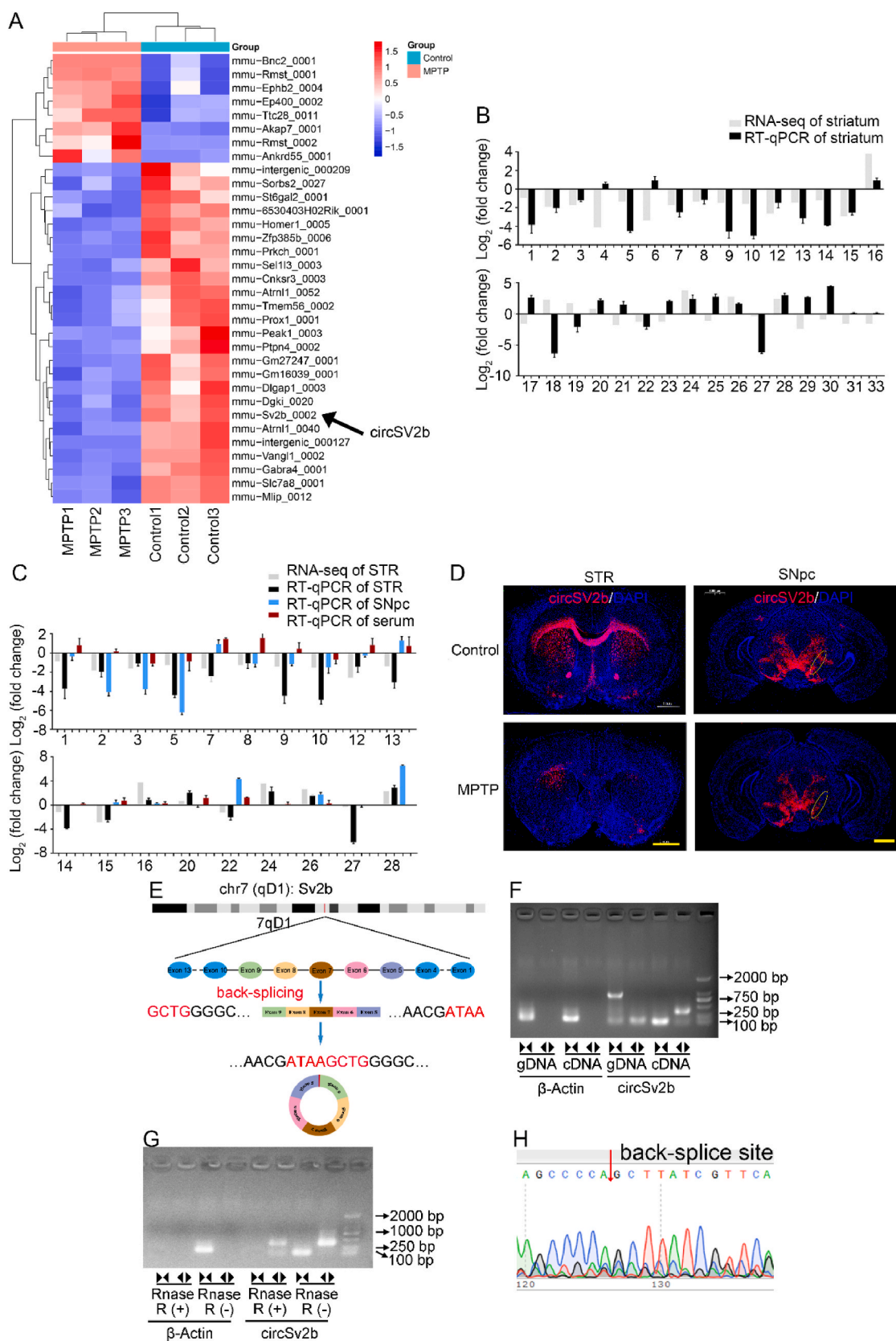


Fig. 2. CircRNA profile analysis in MPTP-induced PD mice. **A** Heatmap of DEGs of MPTP induced PD mice and control mice. **B** Sequencing of circRNA was compared with qRT-PCR results in STR. **C** CircRNA sequencing in STR was compared with qRT-PCR results in STR, SNpc, and serum. **D** Representative photomicrographs of TH staining in STR and SNpc. Scale bars 1000 μm. **E** Genomic loci of *circSV2b* gene. *circSV2b* is produced at the *Sv2b* gene locus. **F** RT-PCR validated the existence of *circSV2b* in SNpc of mice. *circSV2b* was amplified by divergent primers in cDNA (320bp) but not gDNA. β-Actin was used as a negative control. **G** The expression of *circSV2b* in SNpc of mice was detected by PCR assay followed by nucleic acid electrophoresis in the presence or absence of RNase R. **H** We confirmed the head-to-tail splicing of *circSV2b* in the *circSV2b* RT-PCR product by Sanger sequencing.

cDNA, and a 950-bp product was detected in the extracted gDNA (Fig. 2F). Stability is one of the most important characteristics of circRNAs [28]. We used RNase R to verify the stability of circSV2b. First, PCR and agarose gel electrophoresis were performed using specially designed divergent primers and convergent primers. It was found that circSV2b was resistant to RNase R digestion and that linear SV2b and β -actin were not (Fig. 2G). circSV2b cDNA PCR products were subjected to Sanger sequencing (Fig. 2H). The sequences and splicing sites of the PCR products were consistent with their predicted sequences.

3.3. Overexpression of circSV2b improves MPTP-induced PD symptoms in mice

To evaluate the protective effect of circSV2b overexpression on PD, we divided the mice into 4 groups (Fig. S4A), followed by AAV injection, behavioral experiments, and MPTP injection. The efficiency of AAV transfection into the mouse SNpc was verified before the formal experiment (Fig. S4B). qRT-PCR using SNpc tissue showed that the injection of AAV resulted in circSV2b overexpression and that circSV2b expression remained high after MPTP treatment (vs. AAV-ZsGreen + MPTP, $P < 0.01$, Fig. 3A). Both pole-climbing experiments and gait analysis revealed that circSV2b overexpression alleviated impaired motor balance (Fig. 3B). circSV2b overexpression partially restored the DA levels and TH protein levels reduced by MPTP in the SNpc and STR ($P < 0.05$, Fig. 3C–E). The decrease in the number of TH⁺ neurons in the SNpc and the density of STR TH⁺ fibers was also reversed by circSV2b overexpression ($P < 0.05$, Fig. 3F and G). These results indicate that circSV2b overexpression restores dopamine synthesis, maintains nigrostriatal function, and improves the motor function of MPTP-induced PD mice.

3.4. CircSV2b functions through the ceRNA mechanism

CircRNAs play a variety of functions, e.g., molecular sponges of miRNAs, templates for translation, participants in the regulation of translation, and participants in RNAP II extension and variable splicing [29]. The molecular sponge of miRNA is the main way for circRNA, localized to the cytoplasm, to function [30,31]. To explore the subcellular localization of circSV2b, we performed FISH staining using N2A cells and demonstrated that circSV2b was located in the cytoplasm of N2A cells (Fig. 4A). We then tested it at the tissue level. SNpc tissue was subjected to nucleocytoplasmic separation, followed by qRT-PCR. The results indicated that circSV2b was mainly located in the cytoplasm of SNpc, and MPTP treatment resulted in a significant reduction in cytoplasmic circSV2b ($P < 0.01$, Fig. 4B). To act as a molecular sponge, circRNA must form an RNA-induced silencing complex (RISC) with miRNA and AGO2 protein [32]. To prove the binding effect of circSV2b and AGO2, we performed a fluorescent co-labeling experiment. The results showed that circSV2b and AGO2 colocalized (Fig. 4C). The finding provided a spatial basis for the binding of these 2 molecules. The overlapping results of 3 circRNA-miRNA prediction tools (miRanda, TargetScan, and RNAhybrid) were analyzed, and 13 miRNAs were identified (Fig. 4D). The miRTarBase tool was used to predict miRNA target genes; only 3 candidate miRNAs had downstream target genes (Fig. 4E). We compared the levels of candidate miRNAs in SNpc tissue after MPTP treatment. The results showed that compared with that in other candidate miRNAs, the increase in miR-5107-5p was more significant in the MPTP group ($P < 0.01$, Fig. 4F). An anti-AGO2 antibody and a circSV2b probe were further used to perform RIP and RNA pull-down assays, respectively. The anti-AGO2 antibody pulled down circSV2b ($P < 0.01$, Fig. 4G). Moreover, the effect was more obvious in the presence of miR-5107-5p ($P < 0.01$, Fig. 4G). And the circSV2b probe pulled down AGO2 protein (Fig. 4H). The above results indicate that circSV2b functions as a molecular sponge of miRNAs.

Because previous studies have confirmed that Foxk1 is regulated by lncRNA through the ceRNA mechanism [20,21,33], Foxk1 was selected as a downstream molecule among the predicted target genes of

miR-5017-5p. We conducted experiments to verify the expression of Foxk1 in the SNpc. The results indicated that Foxk1 was expressed in the SNpc and colocalized with TH (Fig. S5). Considering that circRNAs, miRNAs, and AGO2 form the RISC, we fluorescently labeled N2A cells to observe the subcellular colocalization of the three molecules. In our study, most circSV2b, miR-5107-5p, and AGO2 colocalized in the cytoplasm (Fig. 4I). We also performed fluorescent labeling experiments to assess the binding of miR-5107-5p and Foxk1 and found that the 2 molecules colocalized in the cytoplasm (Fig. 4J). Because the binding of miRNAs to mRNAs also depends on AGO2 [34], we further performed an RNA pull-down assay using a Foxk1 probe and found that Foxk1 and AGO2 bind (Fig. 4K).

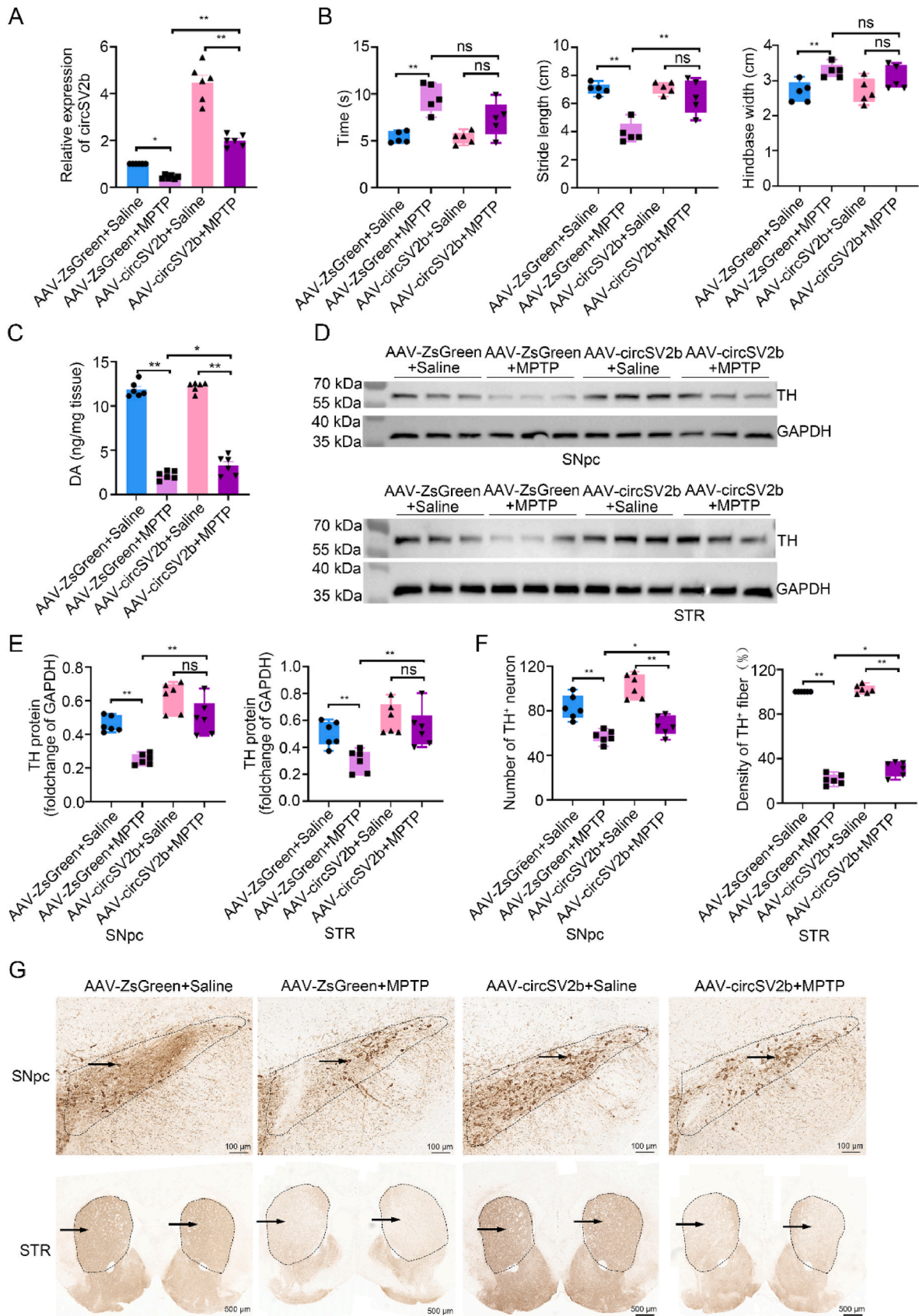
To confirm the bioinformatics prediction analysis, dual-luciferase reporter assay was applied in N2A cells. The full-length of circSV2b-wt (or Foxk1 3'UTR) and mutant version without miR-5107-5p binding sites were subcloned into psiCHECK2 plasmids (Fig. 4L). CircSV2b-wt, circSV2b-mut, and empty vectors were cotransfected with miR-5107-5p mimics, miR-5107-5p inhibitor, or NC into N2A cells to determine the interaction between miR-5107-5p and circSV2b. The results showed that the activity of luciferase transfected with circSV2b-wt significantly decreased in the miR-5107-5p mimics group and increased in the miR-5107-5p inhibitor group ($P < 0.01$, Fig. 4M). However, these effects were not observed with the empty vector and circSV2b-mut (Fig. 4M). Foxk1-wt, Foxk1-mut, and empty vectors were cotransfected with miR-5107-5p mimics, miR-5107-5p inhibitor, or NC into N2A cells to determine the interaction between miR-5107-5p and mRNA Foxk1. The results showed that the activity of luciferase transfected with Foxk1-wt significantly decreased in the miR-5107-5p mimics group and increased in the miR-5107-5p inhibitor group ($P < 0.01$, Fig. 4N). However, these effects were not observed with the empty vector and Foxk1-mut. The above results indicated that circSV2b interacts with miR-5107-5p, and miR-5107-5p interacts with mRNA Foxk1.

3.5. Foxk1 is a transcription factor for Akt1

Because of the important role of oxidative stress in the pathogenesis of PD [22,35], we used CUT & Tag-seq to screen target genes related to oxidative stress downstream of Foxk1. This experiment was double-replicated, and quality assessments and quality control of the data for the 2 samples were assessed (Figs. S6A–E). There were 8013 overlapping peaks (Fig. S6F). We performed gene annotation for the genes associated with the peaks (genes with the transcription initiation site (TTS) closest to the peak) and performed Gene Ontology (GO) annotation and enrichment analysis of peak-associated genes (Fig. 5A and B). Regarding GO, both samples were enriched in “oxidative stress response”. In this GO item, the peak detection results for Akt1 were selected for visualization; the corresponding peaks in the 2 samples were very close to the TTS of Akt1 (Fig. 5C). We compared the sequence of the target peak with the Foxk1 motif and found that they were consistent (Fig. 5D).

3.6. CircSV2b regulates the expression of miR-5107-5p, miR-5107-5p affects the expression of Foxk1, and Foxk1 affects the expression of Akt1

To further explore the regulatory role of ceRNA-Akt1, we performed gene editing experiments using N2A cells. We designed a circSV2b overexpression plasmid and sequenced positive clones to confirm that the sequences in the clones were consistent with the circSV2b sequence (Fig. S7A). The qRT-PCR results confirmed successful circSV2b overexpression ($P < 0.01$, Fig. 6A). qRT-PCR revealed that after circSV2b overexpression, miR-5107-5p and Foxk1 expression was downregulated and upregulated, respectively ($P < 0.01$, Fig. 6A). WB analysis showed that after circSV2b overexpression, both Foxk1 and Akt1 were upregulated ($P < 0.01$, Fig. 6B and C). We designed 3 circSV2b interference plasmids and sequenced shRNAs to confirm that their sequences were consistent with expectations (Fig. S7B). The qRT-PCR results confirmed



(caption on next page)

Fig. 3. Neuroprotective effects of up-regulation of circSV2b in MPTP-induced PD mouse model. **A** Level of circSV2b in SNpc. In AAV-circSV2b + MPTP group, circSV2b expression remained high after MPTP treatment (vs. AAV-ZsGreen + MPTP, $P < 0.01$). Data are mean \pm s.e.m.; $n = 6$. **B** Time to descend pole, stride length, and hindbase width of gait analysis. These results revealed that circSV2b overexpression alleviated impaired motor balance. Data are mean \pm s.e.m.; $n = 6$. **C** The content of DA in STR. CircSV2b overexpression restored the DA levels reduced by MPTP ($P < 0.05$). The result is the amount of DA per mg of tissue. Data are mean \pm s.e.m.; $n = 6$. **D** Representative immunoblots of TH and GAPDH levels in SNpc or STR. **E** Quantification of immunoblots of TH levels in SNpc or STR. CircSV2b overexpression restored the TH levels reduced by MPTP ($P < 0.01$). Data are mean \pm s.e.m.; $n = 6$. **F** Unbiased stereological counts of TH⁺ neurons in SNpc and the quantity of TH⁺ striatal fiber density in STR. Data are mean \pm s.e.m.; $n = 6$. **G** Representative TH staining of SNpc and STR. The black arrows indicate the location of TH⁺ fibers or TH⁺ neurons. Scale bar, 100 μ m for SNpc, 500 μ m for STR. The one-way ANOVAs were used for statistical analysis followed by Bonferroni's post hoc test. * $P < 0.05$, ** $P < 0.01$, ^{ns} $P > 0.05$.

that the interference effect of shRNA1 was the most significant ($P < 0.01$, Fig. 6D). qRT-PCR also revealed that after circSV2b interference, miR-5107-5p and Foxk1 expression was upregulated and downregulated, respectively ($P < 0.01$, Fig. 6E). WB analysis showed that after circSV2b interference, both Foxk1 and Akt1 were downregulated ($P < 0.01$, Fig. 6F and G).

After miR-5107-5p mimics transfection, Foxk1 and Akt1 mRNA and protein expression were downregulated ($P < 0.01$, Fig. 7A–C). The transfection of the miR-5107-5p inhibitor upregulated Foxk1 and Akt1 mRNA and protein expression ($P < 0.01$, Fig. 7D–F).

We designed a Foxk1 overexpression plasmid, sequenced positive clones, and confirmed that the sequences in clones were consistent with the Foxk1 sequence (Fig. S7C). The WB results indicated that Foxk1 was successfully overexpressed and that Akt1 expression was upregulated ($P < 0.01$, Fig. 7G and H). We designed 3 Foxk1 interference plasmids and sequenced shRNAs to confirm that their sequences were consistent with expectations (Fig. S7D). The WB results indicated that shRNA3 had the best interference effects ($P < 0.01$, Fig. 7I and J); therefore, it was selected for subsequent experiments; additionally, after Foxk1 expression interference, the expression of both Foxk1 and Akt1 was downregulated ($P < 0.01$, Fig. 7K and L).

3.7. circSV2b overexpression resists oxidative stress damage in PD through the ceRNA-Akt1 pathway

To explore the mechanism by which circSV2b overexpression leads to resistance to PD, we used MPTP to create a PD mouse model 21 days after AAV injection. The changes in expression of various molecules in the ceRNA-Akt1 pathway and oxidative stress molecules were assessed. The results indicated that circSV2b overexpression reversed the increase of miR-5107-5p caused by MPTP and alleviated the reduction in Foxk1 and Akt mRNA and protein expression ($P < 0.05$, Fig. 8A and B). CircSV2b overexpression reduced the increase in the oxidation product MDA caused by MPTP ($P < 0.01$, Fig. 8C) and also enhance the activity of antioxidant enzymes (SOD and GSH-PX) ($P < 0.05$, Fig. 8D).

As the diagram illustrates in Fig. 9, our findings suggest that circSV2b overexpression protects against the neurodegeneration of dopaminergic neurons and oxidative stress injury in SNpc under the conditions of MPTP. The neuroprotective effects of circSV2b overexpression in PD may be mainly mediated by miR-5107-5p-Foxk1-cAkt1 axis. Moreover, circSV2b can be transported to peripheral blood through exosomes, and its level changes can be detected in serum exosomes of the PD model. Collectively, we demonstrate that circSV2b can be used as a biomarker for the diagnosis of PD. In addition, the favorably neuroprotective effects of circSV2b overexpression render it a promising target in the treatment of PD.

4. Discussion

In this study, in an MPTP-induced PD mouse model, circSV2b expression in SNpc, STR, and serum exosomes was significantly reduced. Additionally, circSV2b overexpression protected against dopaminergic neuron loss maintained nigrostriatal function and alleviated oxidative stress damage. Therefore, circSV2b can be used as a novel target for PD diagnosis and treatment.

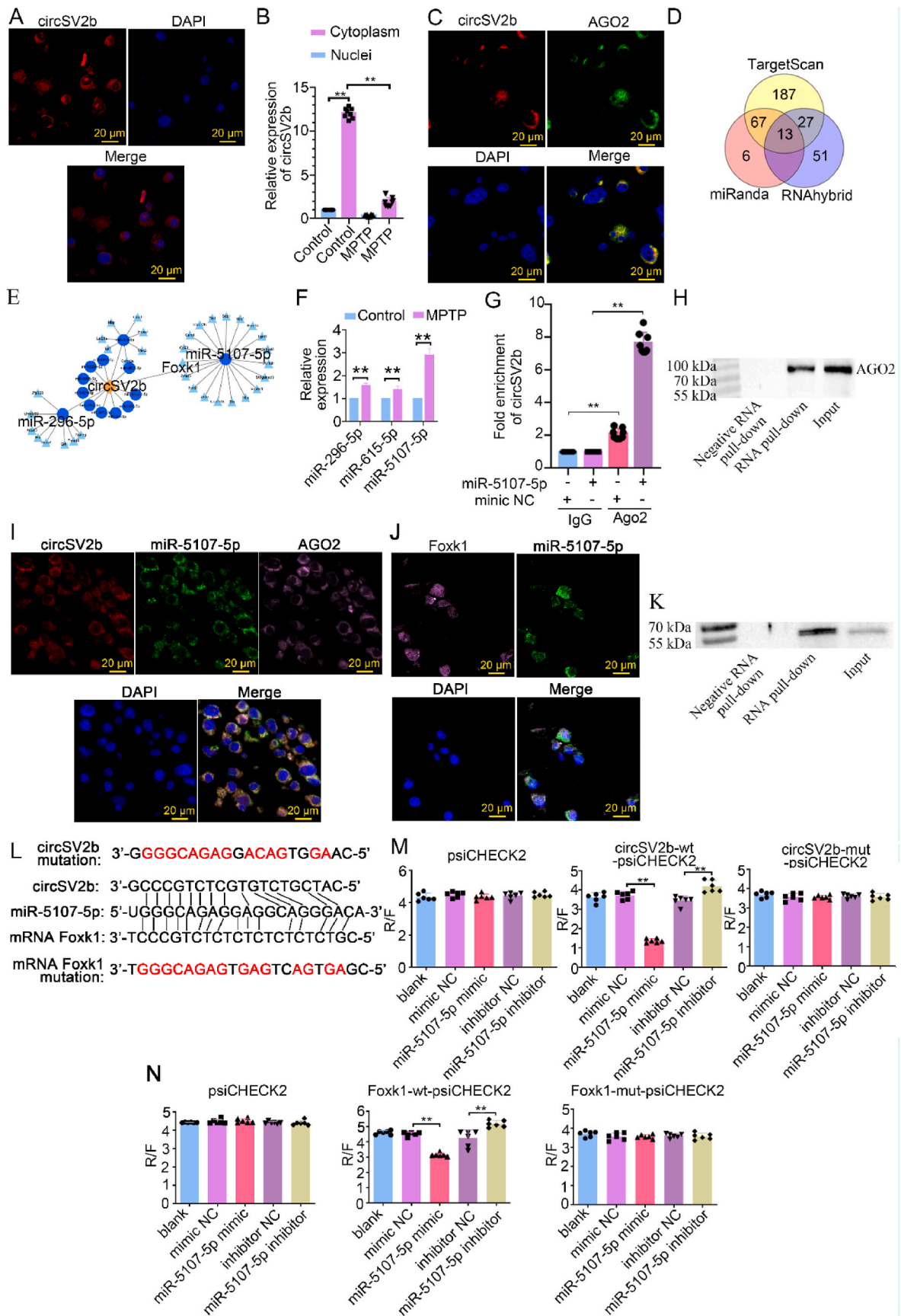
The discovery and study of PD-associated circRNAs provides a

theoretical basis for the study of the mechanism of PD occurrence and development, and provides novel ideas for the diagnosis and treatment of PD [36–39]. Using exosomes, circRNAs can cross the blood–brain barrier to enter the bloodstream and stably exist in the peripheral blood [10,40]. Therefore, circRNAs released from brain and nerve tissue lesions can be detected in peripheral blood. Because blood and cell specimens are easier to obtain than pathological samples from brain tissue, circRNA detection in peripheral blood is of great significance because it can be utilized as a noninvasive approach to assist in disease diagnosis and treatment. If DECs can be identified in body fluids, new approaches for the diagnosis, pathogenesis exploration, and treatment of PD are feasible. Using SNpc and STR sequencing big data, this study assessed circRNA expression in peripheral blood exosomes to screen circRNAs that can be used for diagnosis. Additionally, an in-depth exploration of the molecular mechanism of circRNA involvement in PD was carried out to better understand the pathogenesis of PD and provide a basis for the development of novel therapeutic targets.

CircRNAs are highly expressed in the mammalian brain, and most studies on circRNAs related to neurodegenerative diseases have focused on AD [41–43]. Some studies have found that the level of only a small number of circRNAs in the PD brain changes [38]; however, due to sequencing technology and analysis method limitations, the identification of DECs is limited. Paired-end sequencing of rRNA-depleted RNA, which was used in this study, and the development of related algorithms provide the ability to identify new DECs. In this study, we used paired-end sequencing to process brain tissue samples. Compared with single-end sequencing, paired-end sequencing greatly reduced the error of the sequence reply and improved the quality of the read sequence. For the identification of DECs, we used both the traditional CIRI2 and CIRCexplorer2 software and the previously self-developed DEBKS software to analyze the sequencing data. Twenty-five downregulated and 8 upregulated DECs were found in the STR tissue of MPTP-induced PD mice, but no DECs were found in the SNpc. The sequencing results for the STR were verified by qRT-PCR in STR, SNpc, and serum exosomes. We, finally, focused on circSV2b, which was downregulated at all sites.

The SNpc is particularly important in PD because it associates with the characteristic symptoms of PD caused by the loss of dopaminergic neurons [44,45]. Interestingly, we did not find DECs when analyzed the SNpc sequencing data. We speculate that there was not enough SNpc tissue to meet the sequencing requirements; therefore, risk sequencing was performed. Most of the nerve fibres in the STR come from dopaminergic neuron projections of the SNpc (Fig. S8); therefore, some pathological changes in the STR are the continuation of the SNpc. The sequencing results of the STR were sequentially validated in STR, SNpc, and serum exosomes, and molecules with consistent and obvious expression changes were screened as diagnostic and therapeutic targets. Using exosomes as transporters, circRNAs can cross the blood–brain barrier and reach and stably exist in the peripheral bloodstream, serving as potential novel diagnostic molecules. Compared with the hysteresis of imaging diagnoses and the invasiveness of CSF examinations, peripheral blood tests can be used for screening and are less invasive.

AGO2 is an indispensable molecule in the formation of RISCs [46, 47]. Analysis of circSV2b showed that it is localized in the cytoplasm and binds AGO2. We speculated that circSV2b plays its role through the ceRNA mechanism. Using bioinformatics analysis and preliminary validation, we confirmed the hypothetical connection between circSV2b



(caption on next page)

Fig. 4. CeRNA prediction and targeting validation of circSV2b. **A** FISH assay showed that circSV2b was predominantly localized in the cytoplasm. Scale bars 20 μ m. **B** Levels of circSV2b in the nuclear and cytoplasmic fractions of SNpc detected by qRT-PCR. CircSV2b was mainly expressed in the cytoplasm, and the level of circSV2b in the cytoplasm decreased significantly after MPTP treatment. Data are mean \pm s.e.m.; n = 6. **C** CircSV2b FISH and AGO2 IF assay showed the co-location of circSV2b and AGO2 in the cytoplasm. Scale bars 20 μ m. **D** Schematic illustration exhibiting overlapping of the target miRNAs of circSV2b predicted by TargetScan, RNAhybrid, and miRanda. **E** Target genes of 13 candidate miRNAs predicted by miRTarBase. **F** Relative expression of candidate miRNAs in SNpc. After MPTP treatment, the change of miR-5107-5p was most obvious. Data are mean \pm s.e.m.; n = 6. **G** Anti-AGO2 RIP assay was executed in N2A cells after transfection with miR-5107-5p mimic and NC, followed by qRT-PCR to detect circSV2b. Data are mean \pm s.e.m.; n = 7. **H** CircSV2b pull-down assay was executed in N2A cells, followed by WB to detect the enrichment of AGO2. **I** CircSV2b and miR-5107-5p FISH and AGO2 IF assay showed the co-location of circSV2b miR5107-5p and AGO2 in the cytoplasm. Scale bars 20 μ m. **J** Foxk1 and miR-5107-5p FISH assay showed the co-location of Foxk1 and miR5107-5p in the cytoplasm. Scale bars 20 μ m. **K** mRNA Foxk1 pull-down assay was executed in N2A cells, followed by WB to detect the enrichment of AGO2. **L** Schematic illustration of circSV2b-wt, circSV2b-mut, Foxk1-wt and Foxk1-mut luciferase reporter vectors. **M** The relative luciferase activities were detected in N2A cells after co-transfection with empty vector, circSV2b-wt or circSV2b-mut and mimics, inhibitor or NC, respectively. The activity of luciferase transfected with circSV2b-wt significantly decreased in the miR-5107-5p mimics group and increased in the miR-5107-5p inhibitor group ($P < 0.01$). Data are mean \pm s.e.m.; n = 6. **N** The relative luciferase activities were detected in N2A cells after co-transfection with empty vector, Foxk1-wt or Foxk1-mut and mimics, inhibitor or NC, respectively. The activity of luciferase transfected with Foxk1-wt significantly decreased in the miR-5107-5p mimics group and increased in the miR-5107-5p inhibitor group ($P < 0.01$). Data are mean \pm s.e.m.; n = 6. The one-way ANOVAs were used for statistical analysis followed by Bonferroni's post hoc test. $**P < 0.01$.

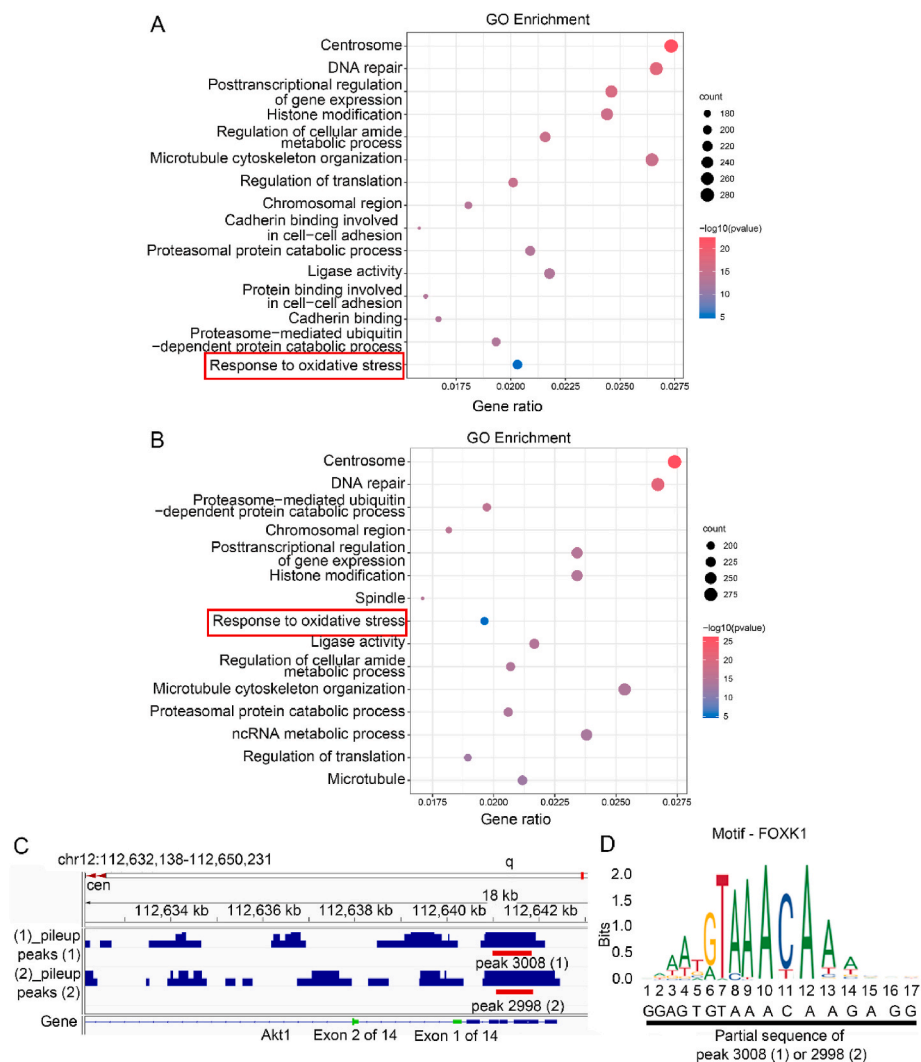


Fig. 5. Target genes of Foxk1 screened by CUT&Tag. **A B** GO analysis for the samples 1 and 2 respectively. The red boxes showed the oxidative stress response. **C** The location of *Akt1*-related peaks and *Akt1* in the genome. **D** Sequence comparison of Foxk1 motif and *Akt1* related peaks. (For interpretation of the references to color in this figure legend, the reader is referred to the Web version of this article.)

and miR-5107-5p, but this speculation could not explain the actually targeted binding and regulatory effect between the two molecules. Many studies have found that lncRNAs regulate Foxk1 expression through the ceRNA mechanism [33,48]. Therefore, we focused on Foxk1 in the downstream predicted target transcripts of miR-5107-5p. Foxk1 mainly plays a role in cell proliferation, differentiation, and regeneration [17,

49,50]. Therefore, studies have mostly focused on auxanology and oncology; there is no report on Foxk1 expression in normal SNpc. The experimental results herein showed that Foxk1 was expressed in normal SNpc and dopaminergic neurons. This finding was a prerequisite for testing the hypothesis of this study. Further experiments found evidence of targeted binding of circSV2b to miR-5107-5p and miR-5107-5p to

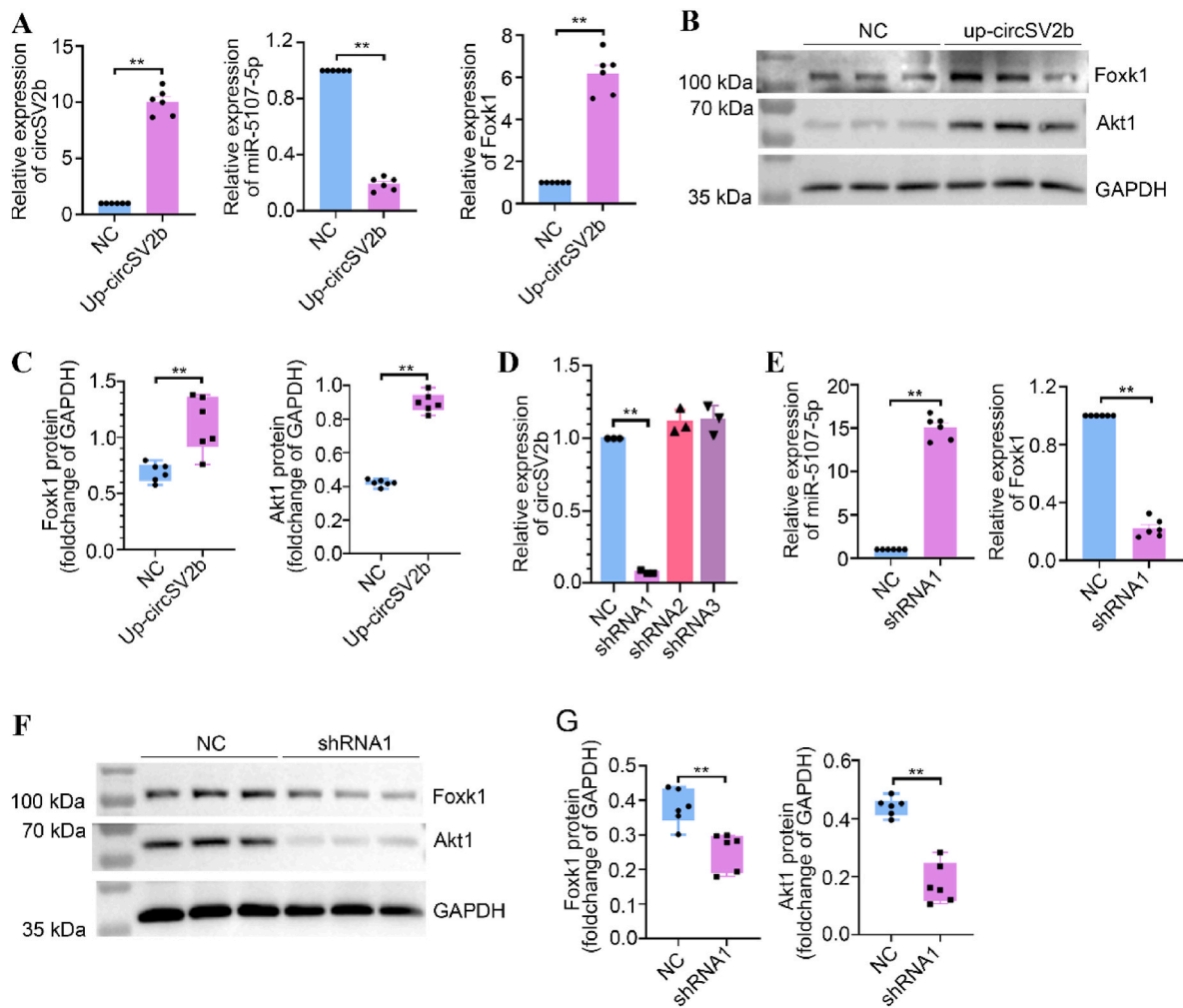


Fig. 6. The level of miR-5107-5p is regulated by circSV2b. **A** After up-regulated circSV2b, relative expression of circSV2b, miR-5107-5p, and Foxk1 in N2A cells was detected by qRT-PCR. The expression of circSV2b and mRNA Foxk1 in up-circSV2b group increased, but miR-5107-5p expression was decreased ($P < 0.01$). Data are mean \pm s.e.m.; $n = 6$. **B C** Representative immunoblots and quantification of relative protein levels of Foxk1 and Akt1 in up-circSV2b N2A cells. The expression of Foxk1 and Akt1 in up-circSV2b group increased ($P < 0.01$). Data are mean \pm s.e.m.; $n = 6$. **D** After transfection with circSV2b shRNAs or NC plasmids, the level of circSV2b was detected by qRT-PCR. The interference effect of shRNA1 was the most significant ($P < 0.01$). **E** After down-regulated circSV2b, relative expression of miR-5107-5p and Foxk1 in N2A cells was detected by qRT-PCR. The expression of miR-5107-5p in shRNA1 group increased, but mRNA Foxk1 expression was decreased ($P < 0.01$). Data are mean \pm s.e.m.; $n = 6$. **F G** Representative immunoblots and quantification of relative protein levels of Foxk1 and Akt1 in down-circSV2b N2A cells. The expression of Foxk1 and Akt1 in shRNA1 group decreased ($P < 0.01$). Data are mean \pm s.e.m.; $n = 6$. The one-way ANOVAs were used for statistical analysis followed by Bonferroni's post hoc test. ** $P < 0.01$.

mRNA Foxk1 and clarified the binding target. It was confirmed that circSV2b regulated activity of miR-5107-5p and affected its function. In addition, the colocalization of circSV2b, miR-5107-5p, and AGO2 indicated that circSV2b could act as a molecular sponge of miR-5107-5p and competitively bind to it. We also found that miR-5107-5p regulated Foxk1 expression and that Foxk1 mRNA could bind to AGO2 (AGO2 is a necessary medium for mRNA targeted binding to miRNA [34,51]). These results indicated that miR-5107-5p could target and bind to Foxk1 mRNA to inhibit its transcription.

As an important transcription factor, Foxk1 plays a key role in the growth and development, cell differentiation, apoptosis, and immunity through transcriptional regulation and signal transduction pathways [17,52]. However, bioinformatics expression analysis [53] showed that FOXK1 was expressed in poorly differentiated tissues of the brain, eye, heart, lung, and thymus. In adults, FOXK1 is mainly expressed in malignant tissues, especially in brain, colorectal, and lymph node tumors. It has not been reported whether FOXK1 is expressed in the SNpc of normal adults or mice. Our study found that FOXK1 is expressed in the SNpc of normal mice, and it is highly expressed in TH⁺ neurons. This

provides the prerequisite for the study of Foxk1 in non-tumor diseases and also ensures the smooth conduct of subsequent experiments in this study.

Oxidative stress plays an important role in the pathogenesis of PD. The transcriptome sequencing results (Fig. S9) also showed that after MPTP treatment, oxidative stress damage could occur, and related pathways were also enriched in the GO analysis. However, no oxidative stress-related genes have been reported among the downstream target genes of Foxk1. Based on this, we performed CUT & Tag-seq to screen relevant target genes. Among the GO-enriched molecules in the oxidative stress response, we focused on Akt1. Akt1 is a serine/threonine kinase that plays an important role in intracellular signaling pathways. As an important intermediate molecule in the PI3K/Akt signal transduction pathway, Akt1 participates in the metabolism of a variety of intracellular substances, plays an important role in the regulation of multiple cellular responses, and is closely related to oxidative stress, apoptosis, and protein synthesis [54–57]. This study showed that Foxk1 can bind to the upstream TTS of Akt1 to mediate its transcription. In addition, after interference with Foxk1 expression, Akt1 expression was

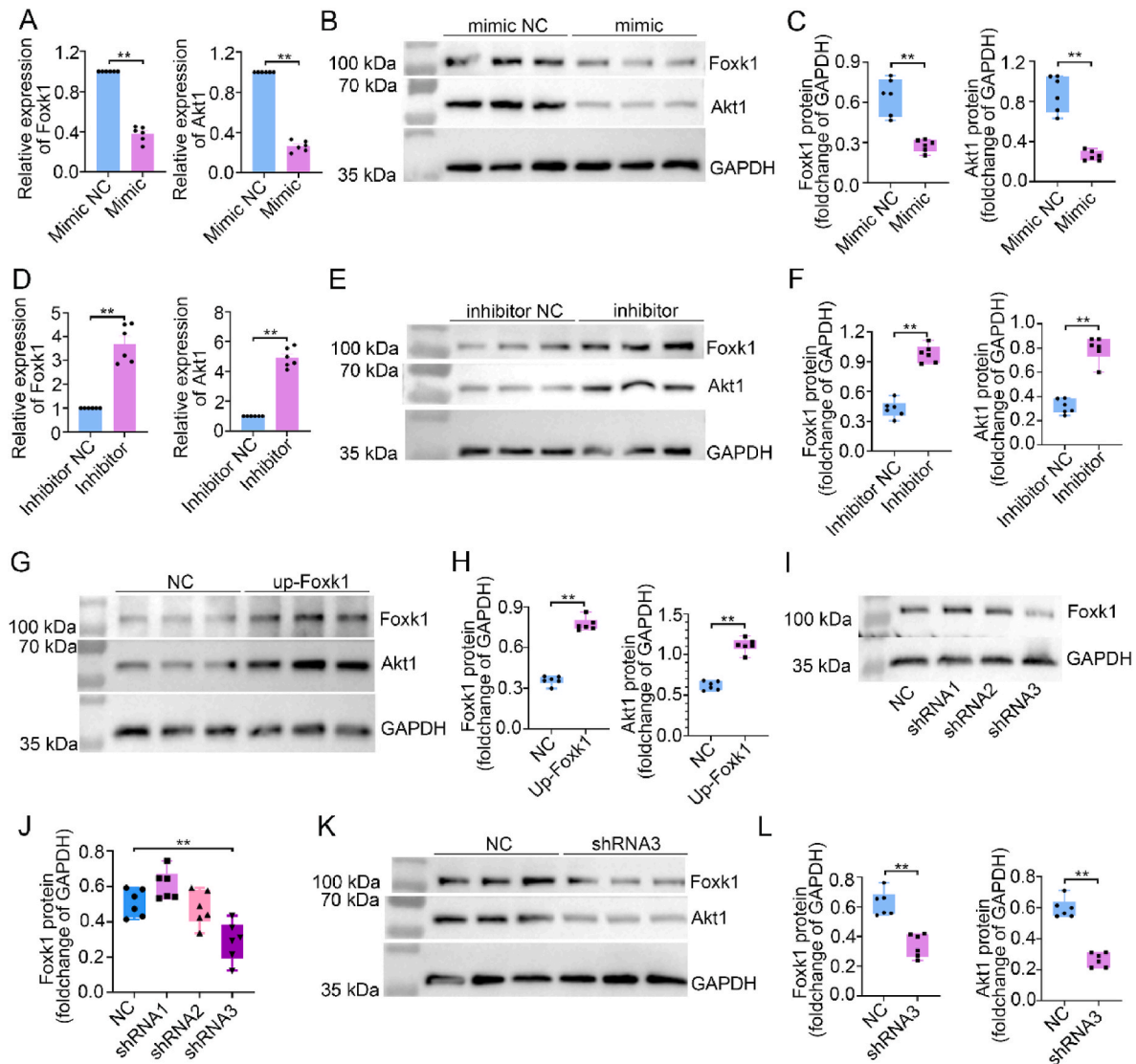


Fig. 7. Foxk1 regulated by miR-5107-5p can regulate Akt1 expression. **A** Relative mRNA levels of Foxk1 and Akt1 were evaluated by qRT-PCR in cells transfected with the miR-5107-5p mimics. **B C** Representative immunoblots and quantification of relative protein levels of Foxk1 and Akt1 in cells transfected with the miR-5107-5p mimics. The expression of Foxk1 and Akt1 in mimic group increased ($P < 0.01$). **D** Relative mRNA levels of Foxk1 and Akt1 were evaluated by qRT-PCR in cells transfected with the miR-5107-5p inhibitor. **E F** Representative immunoblots and quantification of relative protein levels of Foxk1 and Akt1 in cells transfected with the miR-5107-5p inhibitor. The expression of Foxk1 and Akt1 in inhibitor group decreased ($P < 0.01$). **G H** Representative immunoblots and quantification of relative protein levels of Foxk1 and Akt1 in up-Foxk1 cells. The expression of Foxk1 and Akt1 in up-Foxk1 group increased ($P < 0.01$). **I J** Representative immunoblots and quantification of relative protein levels of Foxk1 in cells transfected with Foxk1 shRNAs plasmids. The expression of Foxk1 in shRNA3 group was most significantly decreased ($P < 0.01$). **K L** Representative immunoblots and quantification of relative protein levels of Foxk1 and Akt1 in cells transfected with Foxk1 shRNA3 plasmids. The expression of Foxk1 and Akt1 in shRNA3 group decreased ($P < 0.01$). Data are mean \pm s.e.m.; $n = 6$. The one-way ANOVAs were used for statistical analysis followed by Bonferroni's post hoc test. ** $P < 0.01$.

affected. In the analysis of total motifs and Akt1-peak motifs in the 2 samples (S10-12), multiple Fox family molecules were found, but Foxk1 was not found. We further analyzed the motif of each molecule in the Fox family and found that the Foxk1 motif was relatively complex and might be replaced by other molecules of the same family with similar structures during motif scanning. Sequence analysis also showed that the sequences of the peaks we screened were consistent with the Foxk1 motif. Studies have shown that the nuclear translocation of Foxk1 is regulated by the Akt-mTOR pathway, i.e., Akt promotes the translocation of Foxk1 into the nucleus to function as a transcription factor [58]. In this study, Foxk1 promoted the transcription of Akt1. Therefore, without considering the interference of other factors, Akt1 and Foxk1 formed a closed positive feedback loop.

To date, a variety of methods have been developed for the treatment of PD, for example, drugs, surgery, and cell therapy. However, these

methods are limited to alleviating clinical symptoms and improving the quality of life of patients and cannot fundamentally treat PD [59,60]. Therefore, the development of novel therapeutic targets to prevent or delay the development of PD remains an urgent task. In this study, the results showed that circSV2b overexpression reduced oxidative stress damage, protected against the loss of dopaminergic neurons, maintained nigrostriatal function, and improved motor deficits through the miR-5107-5p-Foxk1-Akt1 signaling pathway. And significant changes in circSV2b could also be detected in serum exosomes. Therefore circSV2b is a promising candidate for PD treatment and helps to provide a better understanding of the pathogenesis of PD. It can also be used as a molecular marker for peripheral blood detection.

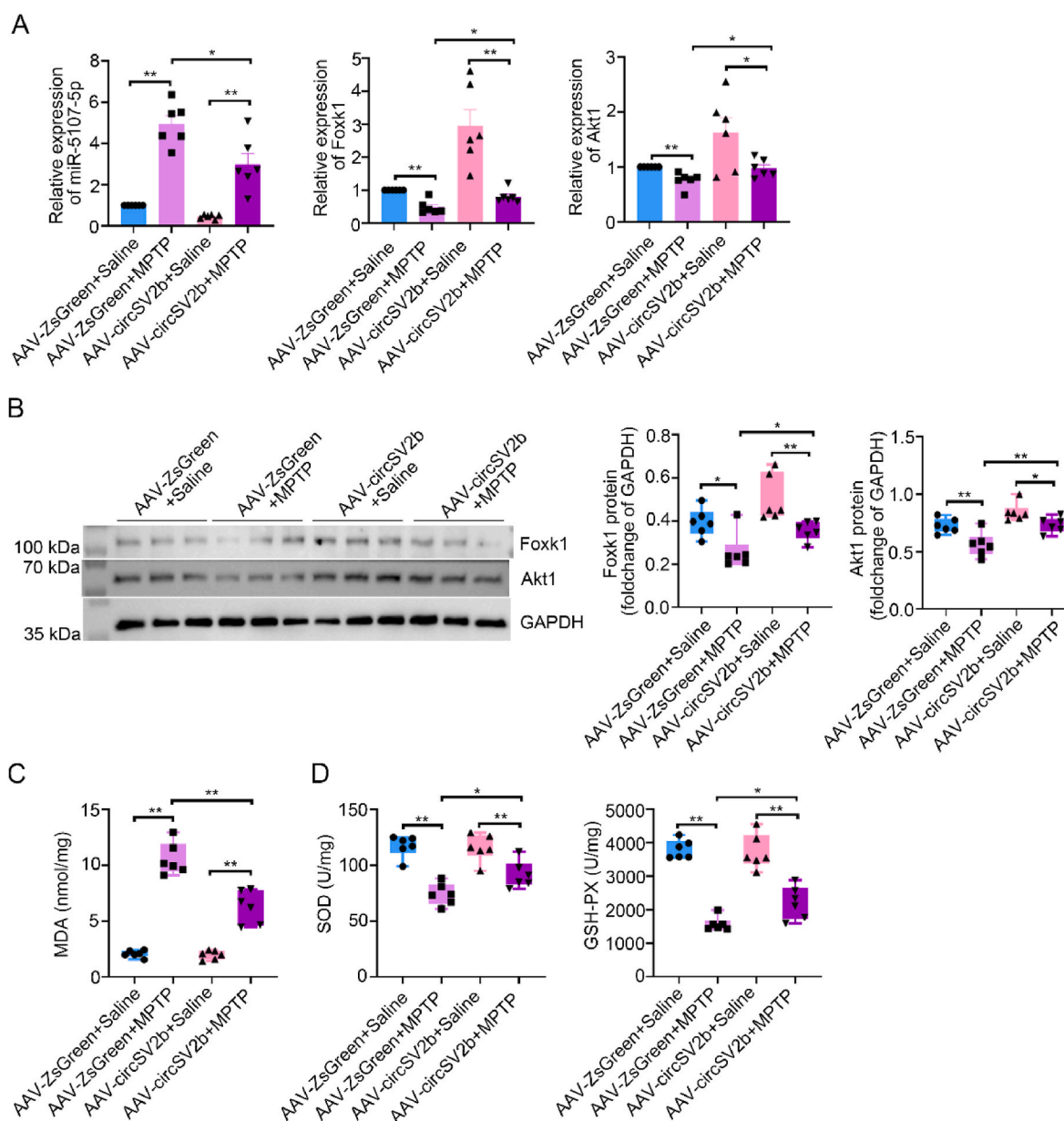


Fig. 8. Up-expression of circSV2b alleviates MPTP-induced oxidative stress injury through ceRNA-Akt1. **A** Relative level of miR-5107-5p, mRNA Foxk1, and Akt1 in SNpc. CircSV2b overexpression alleviated the miR-5107-5p levels elevated by MPTP ($P < 0.05$), and restored the mRNA Foxk1 and Akt1 levels reduced by MPTP ($P < 0.05$). **B** Representative immunoblots and quantification of relative protein levels of Foxk1 and Akt1 in SNpc. CircSV2b overexpression restored the protein Foxk1 and Akt1 levels reduced by MPTP ($P < 0.05$). **C** Levels of MDA in SNpc. CircSV2b overexpression alleviated the MDA levels elevated by MPTP ($P < 0.01$). **D** Levels of SOD and GSH-Px in SNpc. CircSV2b overexpression restored the activity of SOD and GSH-Px reduced by MPTP ($P < 0.05$). Data are mean \pm s.e.m.; $n = 6$. The one-way ANOVAs were used for statistical analysis followed by Bonferroni's post hoc test. * $P < 0.05$, ** $P < 0.01$.

Author contributions

Q.C., C.C and W.Z. designed the study; Q.C., J.W., J.F., H.D., and J.M., carried out experiments; Q.C., J.Z., and H.D. analyzed the data; Q.C., X.F. and H.L. made the figures; Q.C., J.W., M.L., C.C. and W.Z. drafted and revised the paper; all authors approved the final version of the manuscript.

Availability of data and materials

The datasets used and/or analyzed during the current study are included in this article and its supplementary information files. The datasets are available from the corresponding author on reasonable request.

Funding

This work was supported by the National Natural Science Foundation of China (No. 81873769), Human brain bank and regional brain bank collaboration network platform (No. 2021ZD0201100) and the Innovation Fund for Outstanding Doctoral Students (Peking University Health Science Center).

Declaration of competing interest

The authors declare that they have no known competing financial interests or personal relationships that could have appeared to influence the work reported in this paper.

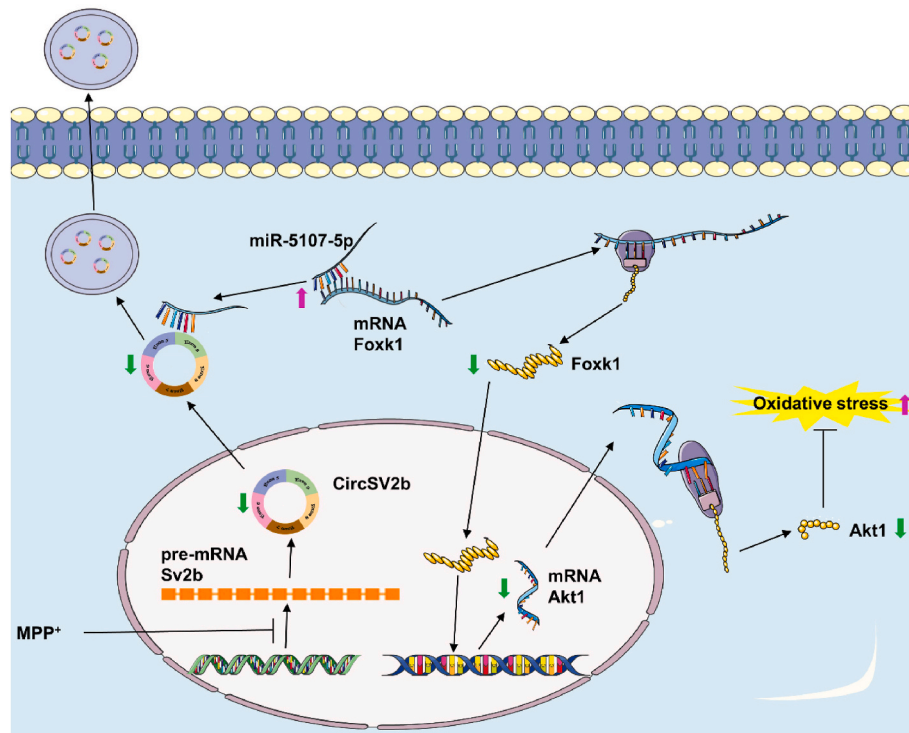


Fig. 9. Schematic summary of the mechanism of circSV2b in MPTP-induced PD.

Data availability

Data will be made available on request.

Acknowledgments

We are very grateful for the help provided by the experiment center for science and technology of Medical and Health Analysis Center, Peking University. We thank Ence Yang (Institute of Systems Biomedicine, Department of Medical Bioinformatics, School of Basic Medical Sciences, Peking University Health Science Center) for technical support.

Appendix A. Supplementary data

Supplementary data to this article can be found online at <https://doi.org/10.1016/j.redox.2022.102430>.

References

- [1] M.T. Hayes, Parkinson's disease and parkinsonism, *Am. J. Med.* 132 (7) (2019) 802–807, <https://doi.org/10.1016/j.amjmed.2019.03.001>.
- [2] L. Leggio, S. Vivarelli, F. L'Episcopo, et al., microRNAs in Parkinson's disease: from pathogenesis to novel diagnostic and therapeutic approaches, *Int. J. Mol. Sci.* 18 (12) (2017), <https://doi.org/10.3390/ijms18122698>.
- [3] K. Wakabayashi, K. Tanji, S. Odagiri, et al., The Lewy body in Parkinson's disease and related neurodegenerative disorders, *Mol. Neurobiol.* 47 (2) (2013) 495–508, <https://doi.org/10.1007/s12035-012-8280-y>.
- [4] X. Wang, S. Yu, F. Li, et al., Detection of alpha-synuclein oligomers in red blood cells as a potential biomarker of Parkinson's disease, *Neurosci. Lett.* 599 (2015) 115–119, <https://doi.org/10.1016/j.neulet.2015.05.030>.
- [5] M. Shi, C.P. Zabetian, A.M. Hancock, et al., Significance and confounders of peripheral DJ-1 and alpha-synuclein in Parkinson's disease, *Neurosci. Lett.* 480 (1) (2010) 78–82, <https://doi.org/10.1016/j.neulet.2010.06.009>.
- [6] L.S. Kristensen, M.S. Andersen, L.V.W. Stagsted, et al., The biogenesis, biology and characterization of circular RNAs, *Nat. Rev. Genet.* 20 (11) (2019) 675–691, <https://doi.org/10.1038/s41576-019-0158-7>.
- [7] X. You, I. Vlatkovic, A. Babic, et al., Neural circular RNAs are derived from synaptic genes and regulated by development and plasticity, *Nat. Neurosci.* 18 (4) (2015) 603–610, <https://doi.org/10.1038/nn.3975>.
- [8] Y. Kitamura, M. Kojima, T. Kurosawa, et al., Proteomic profiling of exosomal proteins for blood-based biomarkers in Parkinson's disease, *Neuroscience* 392 (2018) 121–128, <https://doi.org/10.1016/j.neuroscience.2018.09.017>.
- [9] I.S. Bae, S.H. Kim, Milk exosome-derived MicroRNA-2478 suppresses melanogenesis through the akt-GSK3beta pathway, *Cells* 10 (11) (2021), <https://doi.org/10.3390/cells10112848>.
- [10] D. Xia, X. Gu, Plasmatic exosome-derived circRNAs panel act as fingerprint for glioblastoma, *Aging (Albany NY)* 13 (15) (2021) 19575–19586, <https://doi.org/10.18632/aging.203368>.
- [11] N. Zhang, X. Zhang, W. Xu, et al., CircRNA 103948 inhibits autophagy in colorectal cancer in a ceRNA manner, *Ann. N. Y. Acad. Sci.* 1503 (1) (2021) 88–101, <https://doi.org/10.1111/nyas.14679>.
- [12] L.X. Zhang, J. Gao, X. Long, et al., The circular RNA circHMGB2 drives immunosuppression and anti-PD-1 resistance in lung adenocarcinomas and squamous cell carcinomas via the miR-181a-5p/CARM1 axis, *Mol. Cancer* 21 (1) (2022) 110, <https://doi.org/10.1186/s12943-022-01586-w>.
- [13] Y. Liu, J. Song, H. Zhang, et al., EIF4A3-induced circTOLLIP promotes the progression of hepatocellular carcinoma via the miR-516a-5p/PBX3/EMT pathway, *J. Exp. Clin. Cancer Res.* 41 (1) (2022) 164, <https://doi.org/10.1186/s13046-022-02378-2>.
- [14] Y. Gao, J. Zhang, F. Zhao, Circular RNA identification based on multiple seed matching, *Briefings Bioinf.* 19 (5) (2018) 803–810, <https://doi.org/10.1093/bib/bbx014>.
- [15] X.O. Zhang, R. Dong, Y. Zhang, et al., Diverse alternative back-splicing and alternative splicing landscape of circular RNAs, *Genome Res.* 26 (9) (2016) 1277–1287, <https://doi.org/10.1101/gr.202895.115>.
- [16] Z. Liu, H. Ding, J. She, et al., DEBKS: a tool to detect differentially expressed circular RNA, *Dev. Reprod. Biol.* (2021), <https://doi.org/10.1016/j.gpb.2021.01.003>.
- [17] Y. Liu, W. Ding, H. Ge, et al., FOXK transcription factors: regulation and critical role in cancer, *Cancer Lett.* 458 (2019) 1–12, <https://doi.org/10.1016/j.canlet.2019.05.030>.
- [18] Y. Feng, Z. Bai, J. Song, et al., FOXK1 plays an oncogenic role in the progression of hilar cholangiocarcinoma, *Mol. Med. Rep.* 23 (2) (2021), <https://doi.org/10.3892/mmr.2020.11730>.
- [19] D.J. Garry, G. Maeng, M.G. Garry, Foxk1 regulates cancer progression, *Ann. Transl. Med.* 8 (17) (2020) 1041, <https://doi.org/10.21037/atm-2020-94>.
- [20] F. Gao, Tian J. FOXK1, Regulated by miR-365-3p, promotes cell growth and EMT indicates unfavorable prognosis in breast cancer, *OncoTargets Ther.* 13 (2020) 623–634, <https://doi.org/10.2147/OTT.S212702>.
- [21] S. Zheng, L. Yang, Y. Zou, et al., Long non-coding RNA HUMT hypomethylation promotes lymphangiogenesis and metastasis via activating FOXK1 transcription in triple-negative breast cancer, *J. Hematol. Oncol.* 13 (1) (2020) 17, <https://doi.org/10.1186/s13045-020-00852-y>.
- [22] B.G. Trist, D.J. Hare, K.L. Double, Oxidative stress in the aging substantia nigra and the etiology of Parkinson's disease, *Aging Cell* 18 (6) (2019), e13031, <https://doi.org/10.1111/acel.13031>.

- [23] V. Jackson-Lewis, S. Przedborski, Protocol for the MPTP mouse model of Parkinson's disease, *Nat. Protoc.* 2 (1) (2007) 141–151, <https://doi.org/10.1038/nprot.2006.342>.
- [24] S.P. Yun, T.I. Kam, N. Panicker, et al., Block of A1 astrocyte conversion by microglia is neuroprotective in models of Parkinson's disease, *Nat. Med.* 24 (7) (2018) 931–938, <https://doi.org/10.1038/s41591-018-0051-5>.
- [25] C. Zhang, M. Zhao, B. Wang, et al., The Nrf2-NLRP3-caspase-1 axis mediates the neuroprotective effects of Celastrol in Parkinson's disease, *Redox Biol.* 47 (2021), 102134, <https://doi.org/10.1016/j.redox.2021.102134>.
- [26] E.Y. Huang, T.H. Tsai, T.T. Kuo, et al., Remote effects on the striatal dopamine system after fluid percussion injury, *Behav. Brain Res.* 267 (2014) 156–172, <https://doi.org/10.1016/j.bbr.2014.03.033>.
- [27] Z. Luo, Z. Rong, J. Zhang, et al., Circular RNA circCCDC9 acts as a miR-6792-3p sponge to suppress the progression of gastric cancer through regulating CAV1 expression, *Mol. Cancer* 19 (1) (2020) 86, <https://doi.org/10.1186/s12943-020-01203-8>.
- [28] J.N. Vo, M. Cieslik, Y. Zhang, et al., The landscape of circular RNA in cancer, *Cell* 176 (4) (2019) 869–881, <https://doi.org/10.1016/j.cell.2018.12.021>, e813.
- [29] Y. Geng, J. Jiang, C. Wu, Function and clinical significance of circRNAs in solid tumors, *J. Hematol. Oncol.* 11 (1) (2018) 98, <https://doi.org/10.1186/s13045-018-0643-z>.
- [30] T.B. Hansen, T.I. Jensen, B.H. Clausen, et al., Natural RNA circles function as efficient microRNA sponges, *Nature* 495 (7441) (2013) 384–388, <https://doi.org/10.1038/nature11993>.
- [31] Q. Zheng, C. Bao, W. Guo, et al., Circular RNA profiling reveals an abundant circHIPK3 that regulates cell growth by sponging multiple miRNAs, *Nat. Commun.* 7 (2016), 11215, <https://doi.org/10.1038/ncomms11215>.
- [32] T.B. Hansen, E.D. Wiklund, J.B. Bramsen, et al., miRNA-dependent gene silencing involving Ago2-mediated cleavage of a circular antisense RNA, *EMBO J.* 30 (21) (2011) 4414–4422, <https://doi.org/10.1038/emboj.2011.359>.
- [33] D. Ma, H. Liu, Y. Qin, et al., Circ_0007142/miR-186/FOXK1 axis promoted lung adenocarcinoma progression, *Am. J. Transl. Res.* 12 (8) (2020) 4728–4738.
- [34] Y. Chen, F. Yang, E. Fang, et al., Circular RNA circAGO2 drives cancer progression through facilitating HuR-repressed functions of AGO2-miRNA complexes, *Cell Death Differ.* 26 (7) (2019) 1346–1364, <https://doi.org/10.1038/s41418-018-0220-6>.
- [35] C. Raza, R. Anjum, N.U.A. Shakeel, Parkinson's disease: mechanisms, translational models and management strategies, *Life Sci.* 226 (2019) 77–90, <https://doi.org/10.1016/j.lfs.2019.03.057>.
- [36] E. Jia, Y. Zhou, Z. Liu, et al., Transcriptomic profiling of circular RNA in different brain regions of Parkinson's disease in a mouse model, *Int. J. Mol. Sci.* 21 (8) (2020), <https://doi.org/10.3390/ijms21083006>.
- [37] A. Rybak-Wolf, C. Stottmeister, P. Glazar, et al., Circular RNAs in the mammalian brain are highly abundant, conserved, and dynamically expressed, *Mol. Cell* 58 (5) (2015) 870–885, <https://doi.org/10.1016/j.molcel.2015.03.027>.
- [38] M. Hanan, A. Simchovitz, N. Yayon, et al., A Parkinson's disease CircRNAs Resource reveals a link between circSLC8A1 and oxidative stress, *EMBO Mol. Med.* 12 (9) (2020), e11942, <https://doi.org/10.15252/emmm.201911942>.
- [39] Z. Feng, L. Zhang, S. Wang, et al., Circular RNA circDLGAP4 exerts neuroprotective effects via modulating miR-134-5p/CREB pathway in Parkinson's disease, *Biochem. Biophys. Res. Commun.* 522 (2) (2020) 388–394, <https://doi.org/10.1016/j.bbrc.2019.11.102>.
- [40] A. Chen, L. Zhong, K. Ju, et al., Plasmatic circRNA predicting the occurrence of human glioblastoma, *Cancer Manag. Res.* 12 (2020) 2917–2923, <https://doi.org/10.2147/CMAR.S248621>.
- [41] R. Akhter, Circular RNA and alzheimer's disease, *Adv. Exp. Med. Biol.* 1087 (2018) 239–243, https://doi.org/10.1007/978-981-13-1426-1_19.
- [42] U. Dube, J.L. Del-Aguila, Z. Li, et al., An atlas of cortical circular RNA expression in Alzheimer disease brains demonstrates clinical and pathological associations, *Nat. Neurosci.* 22 (11) (2019) 1903–1912, <https://doi.org/10.1038/s41593-019-0501-5>.
- [43] C. Song, Y. Zhang, W. Huang, et al., Circular RNA Cwc27 contributes to Alzheimer's disease pathogenesis by repressing Pur-alpha activity, *Cell Death Differ.* 29 (2) (2022) 393–406, <https://doi.org/10.1038/s41418-021-00865-1>.
- [44] R. Gordon, E.A. Albornoz, D.C. Christie, et al., Inflammasome inhibition prevents alpha-synuclein pathology and dopaminergic neurodegeneration in mice, *Sci. Transl. Med.* 10 (465) (2018), <https://doi.org/10.1126/scitranslmed.aah4066>.
- [45] D. Matheoud, T. Cannon, A. Voisin, et al., Intestinal infection triggers Parkinson's disease-like symptoms in Pink1(-/-) mice, *Nature* 571 (7766) (2019) 565–569, <https://doi.org/10.1038/s41586-019-1405-y>.
- [46] M. Li, W. Ding, M.A. Tariq, et al., A circular transcript of ncx1 gene mediates ischemic myocardial injury by targeting miR-133a-3p, *Theranostics* 8 (21) (2018) 5855–5869, <https://doi.org/10.7150/thno.27285>.
- [47] C.Y. Yu, T.C. Li, Y.Y. Wu, et al., The circular RNA circBIRC6 participates in the molecular circuitry controlling human pluripotency, *Nat. Commun.* 8 (1) (2017) 1149, <https://doi.org/10.1038/s41467-017-01216-w>.
- [48] J. Liu, J. Zhang, Z. Wang, et al., Knockdown of circALP2 inhibits progression of colorectal cancer by regulating miR-485-5p/FOXK1 Axis, *Cancer Biother. Radiopharm.* 36 (9) (2021) 737–752, <https://doi.org/10.1089/cbr.2019.3310>.
- [49] V. Sukonina, H. Ma, W. Zhang, et al., FOXK1 and FOXK2 regulate aerobic glycolysis, *Nature* 566 (7743) (2019) 279–283, <https://doi.org/10.1038/s41586-019-0900-5>.
- [50] Z.Q. Li, M. Qu, H.X. Wan, et al., FOXK1 promotes malignant progression of breast cancer by activating PI3K/AKT/mTOR signaling pathway, *Eur. Rev. Med. Pharmacol. Sci.* 23 (22) (2019) 9978–9987, https://doi.org/10.26355/eurrev_201911_19564.
- [51] N. Mitash, J.E. Donovan, A. Swiatecka-Urban, The Ago2-miRNA-co-IP assay to study TGF-beta1 mediated recruitment of miRNA to the RISC in CFBE cells, *Jove* (161) (2020), <https://doi.org/10.3791/61571>.
- [52] W. Wang, X. Li, M. Lee, et al., FOXKs promote Wnt/beta-catenin signaling by translocating DVL into the nucleus, *Dev. Cell* 32 (6) (2015) 707–718, <https://doi.org/10.1016/j.devcel.2015.01.031>.
- [53] J.T. Huang, V. Lee, Identification and characterization of a novel human FOXK1 gene in silico, *Int. J. Oncol.* 25 (3) (2004) 751–757.
- [54] P. Abeyrathna, Y. Su, The critical role of Akt in cardiovascular function, *Vasc. Pharmacol.* 74 (2015) 38–48, <https://doi.org/10.1016/j.vph.2015.05.008>.
- [55] J.L. Larson-Casey, J.S. Deshane, A.J. Ryan, et al., Macrophage Akt1 kinase-mediated mitophagy modulates apoptosis resistance and pulmonary fibrosis, *Immunity* 44 (3) (2016) 582–596, <https://doi.org/10.1016/j.immuni.2016.01.001>.
- [56] A.K. Singh, M.P. Kashyap, V.K. Tripathi, et al., Neuroprotection through rapamycin-induced activation of autophagy and PI3K/Akt1/mTOR/CREB signaling against amyloid-beta-induced oxidative stress, synaptic/neurotransmission dysfunction, and neurodegeneration in adult rats, *Mol. Neurobiol.* 54 (8) (2017) 5815–5828, <https://doi.org/10.1007/s12035-016-0129-3>.
- [57] M. Vakili Saatloo, A.A. Aghbali, M. Koohsoltani, et al., Akt1 and Jak1 siRNA based silencing effects on the proliferation and apoptosis in head and neck squamous cell carcinoma, *Gene* 714 (2019), 143997, <https://doi.org/10.1016/j.gene.2019.143997>.
- [58] M. Sakaguchi, W. Cai, C.H. Wang, et al., FoxK1 and FoxK2 in insulin regulation of cellular and mitochondrial metabolism, *Nat. Commun.* 10 (1) (2019) 1582, <https://doi.org/10.1038/s41467-019-09418-0>.
- [59] M.J. Armstrong, M.S. Okun, Diagnosis and treatment of Parkinson disease: a review, *JAMA* 323 (6) (2020) 548–560, <https://doi.org/10.1001/jama.2019.22360>.
- [60] V. Cabreira, J. Massano, [Parkinson's disease: clinical review and update], *Acta Med. Port.* 32 (10) (2019) 661–670, <https://doi.org/10.20344/amp.11978>.